International Geology Review

ISSN: (Print) (Online) Journal homepage: www.tandfonline.com/journals/tigr20

Carboniferous variation of crustal thickness and subduction angles in Eastern Tianshan, NW China: evidence from the petrogenesis of the magmatic rocks in the Aqishan–Yamansu Belt

Bin Wu, Xiaoping Long, Shitao Zhang, Yunying Zhang, Zongying Huang & Long Du

To cite this article: Bin Wu, Xiaoping Long, Shitao Zhang, Yunying Zhang, Zongying Huang & Long Du (2023) Carboniferous variation of crustal thickness and subduction angles in Eastern Tianshan, NW China: evidence from the petrogenesis of the magmatic rocks in the Aqishan–Yamansu Belt, International Geology Review, 65:5, 682-705, DOI: 10.1080/00206814.2022.2059710

To link to this article: https://doi.org/10.1080/00206814.2022.2059710

View supplementary material

Published online: 06 Apr 2022.

Submit your article to this journal

Article views: 394

View related articles

View Crossmark data

Citing articles: 1 View citing articles

Full Terms & Conditions of access and use can be found at
https://www.tandfonline.com/action/journalInformation?journalCode=tigr20

版权所有(C)国家科技图书文献中心

INTERNATIONAL GEOLOGY REVIEW
2023, VOL. 65, NO. 5, 682–705
https://doi.org/10.1080/00206814.2022.2059710

Taylor & Francis
Taylor & Francis Group

Check for updates

Carboniferous variation of crustal thickness and subduction angles in Eastern Tianshan, NW China: evidence from the petrogenesis of the magmatic rocks in the Aqishan–Yamansu Belt

Bin Wu[a], Xiaoping Long[a], Shitao Zhang[a], Yunying Zhang[b], Zongying Huang[c] and Long Du[d]

[a]State Key Laboratory of Continental Dynamics, Department of Geology, Northwest University, 710069 Xi'an, China; [b]Key Laboratory of Ocean and Marginal Sea Geology, South China Sea Institute of Oceanology, Chinese Academy of Sciences, 510301, Guangzhou China; [c]State Key Laboratory of Isotope Geochemistry, Guangzhou Institute of Geochemistry, Chinese Academy of Sciences, Guangzhou, China; [d]Shandong Provincial Key Laboratory of Depositional Mineralization & Sedimentary Minerals, Shandong University of Science and Technology, 266590, Qingdao, China

ABSTRACT

New geochronological and geochemical data were presented for the Early Carboniferous basaltic to andesitic volcanic rocks and Late Carboniferous granitic intrusions in the Aqishan–Yamansu Belt of Eastern Tianshan, NW China. Zircon U–Pb dating indicates that the andesite and granite were emplaced at 330 Ma and 321 Ma, respectively. The andesitic rocks of the Yamansu Formation (FM) display subalkaline to calc-alkaline characteristics with moderate SiO_2, relatively high $Mg^{\#}$ values, and low Cr, Co and Ni, indicating an origin from mantle-derived melts. Their relatively low $\varepsilon_{Nd}(t)$ values (−0.02 ~ +0.61) and old T_{DM} ages (T_{DM} = 1.39–1.40 Ga) suggest a mantle source with addition of old crustal materials. Their high Rb/Y and Ba/La, low Nb/Y and Th/Yb ratios elucidate that the magma sources were probably metasomatized by slab-derived fluids. Besides, the high Th and low Ce/Th and Ba/Th ratios of the andesites suggest a contribution from subducted sediment–derived melts. Integrated with the depletion in high field strength elements and enrichment in light rare earth elements (LREEs), we suggest that the Yamansu andesites were formed by partial melting of relatively enriched mantle wedge metasomatized by both subducted sediment-derived melts and fluids. The basalts of the Tugutublak Formation (TF) have high MgO, $Mg^{\#}$ (56–58) and $\varepsilon_{Nd}(t)$ (+5.9 ~ +6.3) values with enriched in LREEs and depleted in Nb–Ta–Ti anomalies, implying an arc setting. Their high Ba/Th, Ba/La and low Th/Ta, Th/Yb ratios suggest that the slab-derived fluids were involved. The basaltic andesites of the TF have higher SiO_2, lower $Mg^{\#}$ (48–50), Cr, Ni and $\varepsilon_{Nd}(t)$ (+1.21) values than the basalts of this formation, indicating that they were evolved from the basaltic magma. Therefore, the Carboniferous volcanic rocks in this study indicate that the Aqishan–Yamansu Belt was in a subduction background. The granites intruding into the TF show typical characteristics of I-type granite. Their highly positive $\varepsilon_{Hf}(t)$ values (+14 ~ +17) suggest a significant contribution from juvenile basaltic lower crust. Moreover, changes in the Dy/Yb and Ho/Yb ratios of Late Paleozoic felsic igneous rocks in the Aqishan–Yamansu Belt imply that the crust underwent four periods of thickening and thinning, which were likely triggered by the variation of subduction angles.

ARTICLE HISTORY
Received 31 December 2021
Accepted 26 March 2022

KEYWORDS
Central Asian Orogenic Belt; Eastern Tianshan; volcanic rocks; I-type granite; crustal thickness

CONTACT Xiaoping Long longxp@nwu.edu.cn State Key Laboratory of Continental Dynamics, Department of Geology, Northwest University, 710069, Xi'an, China

Supplemental data for this article can be accessed here

© 2022 Informa UK Limited, trading as Taylor & Francis Group

版权所有©国家科技图书文献中心 D240625015535YJ00

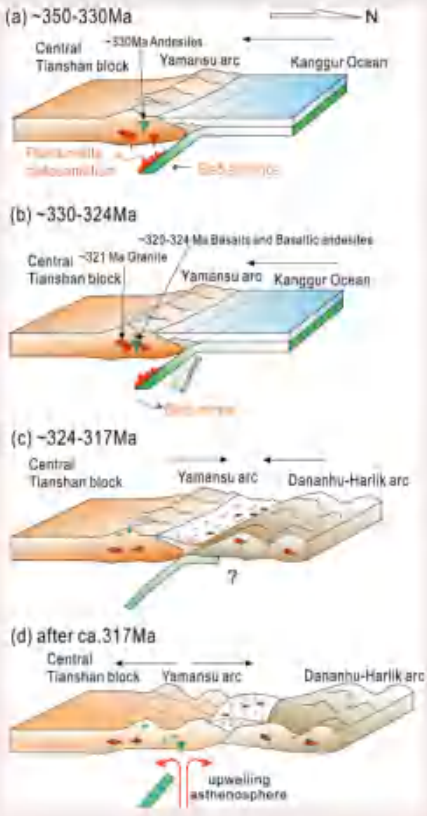

1. Introduction

The Central Asian Orogenic Belt (CAOB, ca. 1000 ~ 250 Ma) also known as the modified Altaids in the literature (Sengör *et al.* 1993; Xiao *et al.* 2015), sandwiched between the Tarim and North China cratons to the south and Baltica and Siberian cratons to the north (Figure 1(a)). The CAOB was formed by convergence of the Kazakhstan, Tarim-North China and Mongolia collage systems, and finally rotated into two major oroclines including the Kazakhstan and Tuva-Mongol in the Carboniferous to Early Permian (Xiao *et al.* 2015, 2018), which has preserved a great deal of evidence related to tectonic evolution and crustal growth during its very long accretion process (Windley *et al.* 2007; Xiao *et al.* 2010, 2015, 2018; Long *et al.* 2012; Xiao and Santosh 2014; Cai *et al.* 2017; Safonova *et al.* 2017; Tang *et al.* 2017; Li *et al.* 2019). The detail processes of accretion and architecture of CAOB are vital to understanding the evolution of the CAOB, and these issues have previously attracted many attentions (e.g. Xiao *et al.* 2004, 2015, 2018; Xiao and Santosh 2014; Safonova *et al.* 2017; Liu *et al.* 2021). The long-lived multi-stage tectonic evolution of the CAOB can be summarized briefly as Proterozoic to Paleozoic accretion and collision, Mesozoic intracontinental modification, and then followed by Cenozoic rapid deformation and uplift (Wang *et al.* 2011). In spite of these achievements, there still have some controversies about the tectonic evolution of the CAOB, such as the subduction direction of different oceanic slabs and the collisional timing among different terranes (Gao *et al.* 2009; Charvet *et al.* 2011; Li *et al.* 2019; Liu *et al.* 2021).

The Tianshan Orogenic Belt (TOB) lies in the southern CAOB, which is the largest Phanerozoic orogenic system on the world (Xia *et al.* 2003; Windley *et al.* 2007; Wilhem *et al.* 2012). Numerous studies show that the TOB was generated by the subduction and closure of Paleo-Asian Ocean and abundant Phanerozoic magmatic rocks were exposed in this orogenic belt, especially the Late Carboniferous to Permian rocks (e.g. Shu *et al.* 2004; Wang *et al.* 2007, 2018; Wu *et al.* 2006; Zhou *et al.* 2010; Zhang et al. 2012a, 2012b; Lei *et al.* 2013; Hou *et al.* 2014; Zheng 2015; Luo *et al.* 2012, 2016; Zhang *et al.* 2016, Zhao et al., 2017; Zhao *et al.* 2018b; Du *et al.* 2018a, 2018b, 2021; Safonova *et al.* 2017; Long *et al.* 2020). Eastern Tianshan, as the eastern segment of the TOB, is mostly covered by the Gobi. It belongs to an accretionary orogen, which comprises accretionary wedge prisms, ophiolitic mélanges, magmatic arcs, and oceanic plateaus and continental remnants (Cawood *et al.* 2009). Researches deduced that slab rollback relative to the

版权所有(c)国家科技图书文献中心 D2406250153SY300

overlying plate and advance marked by advancing of overlying plate are common due to variable angles and velocities of subducted slabs in the accretionary orogens, such as modern western Pacific and Andes (Royden 1993; Collins 2002; Cawood *et al.* 2009). At the same time, some similar researches on the advancing and retreating subduction were carried out in the TOB, such as in the western Tianshan (e.g. Tao *et al.* 2022) and the eastern Tianshan (e.g. Zhang *et al.* 2018, 2019; Du *et al.* 2021). In recent two decades, abundant Carboniferous to Permian volcanic rocks and granitoids were identified within Eastern Tianshan (Wu *et al.* 2006; Zhou *et al.* 2010; Lei *et al.* 2013; Zhang *et al.* 2013; Hou *et al.* 2014; Zheng 2015; Luo *et al.* 2012, 2016; Zhang *et al.* 2016, Zhao et al., 2017; Zhao *et al.* 2018b, 2021; Du *et al.* 2018a, 2018b, 2021; Long *et al.* 2020). These rocks, therefore, can provide important clues to the slab rollback and advance in Eastern Tianshan and its relationship with the tectonic evolution of the whole TOB.

In this study, we focus on the Carboniferous magmatic rocks in the Aqishan–Yamansu Belt of Eastern Tianshan to constrain the variation of slab angle and the subduction and collision processes. New in-situ zircon U–Pb and Hf isotopes, whole-rock major and trace elements and Sr–Nd isotopic data were carried out for the Carboniferous basalts to felsic igneous rocks in the Aqishan–Yamansu Belt. Combined with previous published data, we provide new constraints on the petrogenesis and magma source of these rocks and the relevance slab advance/retreat process in Eastern Tianshan.

2. Geological background

The TOB was characterized by complicated collage of island arc assemblages, remnants of oceanic crust, accretionary wedge prisms and continental remnants (Figure 1(b)) (Windley *et al.* 1990; Allen *et al.* 1993; Xiao *et al.* 2013). It is generally divided into western and eastern parts by the Urumqi–Korla Road. Eastern Tianshan has width of ~300 km, and comprises four sub-units from north to south, including the Dananhu–Harlik Island Arc Belt, the Kanggur Shear Zone, the Aqishan–Yamansu Belt, and the Central Tianshan Block (CTB) (Figure 1(c); (Charvet *et al.* 2007; Xiao *et al.* 2013).

The CTB in Eastern Tianshan is characterized by a Proterozoic (1458–696 Ma) crystalline basement with Early Paleozoic covers (Figure 1(c)). The basement rocks include the Xingxingxia Group and the Kawabulak Group, which mainly consist of silimanite–biotite–quartz schist, granitic gneisses, granulites, amphibolites, migmatites and marbles (Huang *et al.* 2017, 2019). The overlying Early Paleozoic volcanic and sedimentary rocks are composed of the Ordovician calc–alkaline basalt, andesite and greywacke, which are widespread in the CTB (Figure 1c); (Gao *et al.* 1998; Hu *et al.* 2000; Dong *et al.* 2011; Lei *et al.* 2011; He *et al.* 2012; Huang *et al.* 2013, 2017; Xiao *et al.* 2013; Long and Huang 2017). The Ordovician and Silurian volcanic rocks show calc-alkaline geochemical characteristics (Ma *et al.* 1997; Shu *et al.* 1999; Li *et al.* 2008). Recently, zircon U-Pb dating of two subduction-related mafic plutons from the eastern CTB yielded Late Carboniferous ages (~300 Ma), suggesting the Southern Tianshan ocean continued to subduct beneath the CTB in the southern Altaids at this time (Mao *et al.* 2021).

The Kanggur Shear Zone is an accretionary complex with 5 to 24 km wide and ~600 km long (Figure 1(c)). This Zone is characterized by intensive deformation and low-grade metamorphism (Shu *et al.* 1999; Xu *et al.* 2003; Wang *et al.* 2008; Branquet *et al.* 2012). Wang et al. (2014) suggest that the Kanggur Shear Zone experienced dextral strike-slip shearing during the Permian (Branquet *et al.* 2012) with localized thrusting or faulting in response to local transpression or transtension, respectively. This shear zone was composed mainly of ductile deformed and low-grade metamorphosed Carboniferous volcaniclastic, greenschist–facies metamorphosed rocks, and Permian mafic–ultramafic intrusions (Xia *et al.* 2004; Branquet *et al.* 2012). Devonian rocks consist of basalt and andesite with minor rhyolite, dacite, volcanic breccia, tuff and clastic rocks are only occurred to the north of the shear zone (Wan et al., 2014). Furthermore, ophiolitic slices with disconnected formations were also found in the northern part of the Kanggur Shear Zone, which may represent a remnant ocean basin (Xia *et al.* 2004; Li *et al.* 2008; Zhang *et al.* 2016). In addition, the SHRIMP zircon U–Pb dating for gabbros from the ophiolites yielded ages of ~494 to 330 Ma (Li *et al.* 2000, 2008). Their isotopic analysis of Sr–Nd and geochemical data show similar characters to supra-subduction zone–affinity ophiolites (Li *et al.* 2008). Recently, the discovery of the youngest matrix (234 Ma) in the Kanguer accretionary mélange containing blocks of N-MORB basalts indicates a northward subduction of the Paleo-Asian Kanguer Ocean in Eastern Tianshan (Ao *et al.* 2021).

To the north, the Dananhu–Harlik Island Arc Belt is divided into two tectonic units: Dananhu–Harlik arc and Bogda back-arc basin (Figure 1c); (Xia *et al.* 2004; Chen *et al.* 2012). The Dananhu–Harlik arc comprises the Ordovician to Devonian–Carboniferous volcanic rocks, pyroclastic rocks and accretionary complexes (Xiao *et al.* 2004, 2013). The arc-related magmatic rocks are related to the southward Junggar Ocean (e.g. Ma *et al.* 1997; Shu *et al.* 2000; Qin *et al.* 2002; Charvet *et al.* 2011) /Kelamaili Ocean (e.g. Li 2004; Xiao *et al.* 2004, 2009; Li *et*

版权所有©国家科技图书文献中心 D2406250153SY00

al. 2009; Su *et al.* 2012; Mao *et al.* 2016), or the northward subduction of the Kanggur ocean (the east-extending of the North Tianshan Ocean) (Zhang *et al.* 2018; Du *et al.* 2018c; Mao *et al.* 2019). The Bogda back-arc basin contains Carboniferous and Permian sedimentary rocks, such as mudstone, sandstone, siltstone, conglomerate, and limestone (Zhang *et al.* 2018). This basin was resulted from the extension of the Dananhu–Harlik arc in the Late Carboniferous (Zhang *et al.* 2018; Du *et al.* 2018c).

The Aqishan–Yamansu Belt, located between the Kanggur Shear Zone and the CTB, was separated by the Yamansu Fault in the north and Aqikekuduke Faults in the south, respectively (Figure 1(c)). This belt is mainly composed of two marine strata units: Early Carboniferous Yamansu Formation (YF) and Late Carboniferous Tugutublak Formation (TF) (Huang *et al.* 2012; Zhang *et al.* 2016; Zhao et al., 2018a, 2018b; Zhao *et al.* 2021; Du *et al.* 2018a). The YF was exposed in the northern part of the Aqishan–Yamansu Belt and composed of pyroclastic rocks, carbonate deposits and minor volcanic lava (Figure 2). The lithology of the YF can be divided into three members: (i) the bottom, mafic to intermediate-acid tuff, lava breccia and medium-to fine-grained sandstone with minor intercalation of bioclastic limestone; (ii) the middle, limestone (i.e. bioclastic and microcrystalline limestone) with some grey-green volcanic breccia, coarse-grained or coarse-grains-containing sandstone and tuffaceous sandstone (Zhang et al., 2012b); and (iii) the uppermost, limestone, tuff sandstone with minor tuff (Qin *et al.* 2002; Hou *et al.* 2014). The volcanic lavas of the TF are mainly distributed in the southern part of the Aqishan–Yamansu Belt and also can be divided into three sections, i.e. (i) the lower section of fuchsia andesite, rhyolite, crystalline tuff with minor fuchsia tuff and tuff sandstone; (ii) the middle section of sedimentary pyroclastic rocks with bioclastic or bioclastic limestone, volcanic breccia and tuffaceous

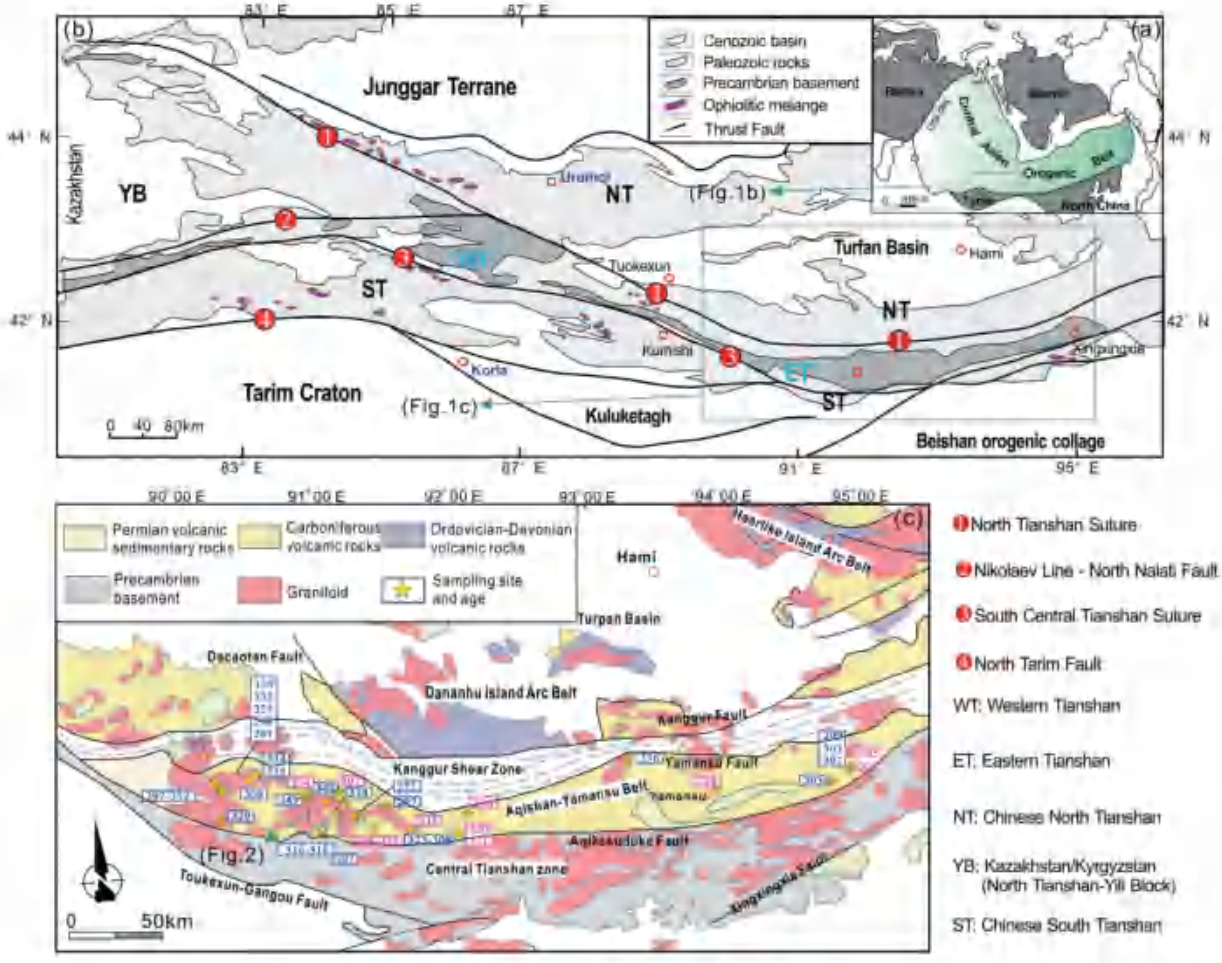

Figure 1. (a) Simplified tectonic map of the CAOB (modified after Jahn *et al.*); (b) Sketch map showing the tectonic framework of Tianshan Belt (simplified after Gao *et al.* 2009); (c) Geological map of Eastern Tianshan (after Zhang *et al.* 2016). Age data (Ma) are from Wang *et al.* (2005), Wu *et al.* (2006), Zhou *et al.* (2010), Hou *et al.* (2014), Zhang *et al.* (2015), Wang *et al.* (2016a, 2016b), Lu *et al.* (2017), Jiang *et al.* (2017), Zhang *et al.* (2016), Zhang *et al.* (2017), Zhao *et al.* (2017), Du *et al.* (2018a) and Zhao *et al.* (2018a, 2018b). Blue data are ages of intrusive rocks, pink data are ages of volcanic rocks.

版权所有(c)国家科技图书文献中心 D240625015355Y100

sandstone; and (iii) the uppermost section of purplish-gray andesite and grey basalt, with minor interlayers of aubergine rhyolite and sandstone (Zhang et al., 2012b; Zhang *et al.* 2016). In addition, the Carboniferous (303–307 Ma, 314–318 Ma and 329–347 Ma) and Permian (243–252 Ma and 272–292 Ma) intrusions are widely developed in the Aqishan-Yamansu Belt (Figure 1(c); (Wu *et al.* 2006; Zhou *et al.* 2010; Lei *et al.* 2013; Zhang *et al.* 2013, 2016; Zheng 2015; Du *et al.* 2018a).

3. Sampling and petrography

The studied samples were collected from the Bailingshan area in the southern part of the Aqishan-Yamansu Belt (Figures 1 and 2). The andesites from the Early Carboniferous YF are greyish-green and dark grey in colour, and display typical porphyritic texture with phenocrysts (~20 vol.%) of clinopyxene and plagioclase, and matrix minerals of plagioclase (Figure 3(a, b)). The basalts from the Late Carboniferous TF show dark-grey in colour with vesicular structure. They consist mainly of clinopyroxene phenocryst (ca. 30 vol.%) and fine columnar-shaped plagioclase (Figure 3(c, d)). The basaltic andesites that collected from the TF also are vesicular structure and have similar mineral assemblages to the above basalts, but with more phenocrysts (~60 vol.%), including euhedral feldspar and granular clinopyroxene (Figure 3(e, f)). The feldspar phenocrysts are dominated by plagioclase. Besides, the matrix of all the above samples is mainly composed of tiny crystals of plagioclase quartz with minor glass. Moreover, the granites from the Bailingshan complex were intruded into the TF and have medium- to coarse-grained granitic texture (Figure 3(g, h)). The granitic rocks contain quartz (~45 vol.%), plagioclase (~35 vol.%), K-feldspar (~10 vol.%), hornblende (~5 vol.%) and biotite (~5 vol.%) with minor accessory minerals of apatite, sphene, zircon and Fe-Ti oxide.

4. Analytical methods and results

Zircon U-Pb dating and in-situ Hf isotopic analyses was carried out at the State Key Laboratory of Continental Dynamics, Northwest University, China. Whole-rock major and trace elements and Sr-Nd isotope analyses were carried out at the State Key Laboratory of Isotope Geochemistry, Guangzhou Institute of Geochemistry and Nanjing FocuMS Technology Co. Ltd., respectively. Detailed analytical methods and procedures are described in the Appendixes and all the analytical results are listed in Supplementary tables.

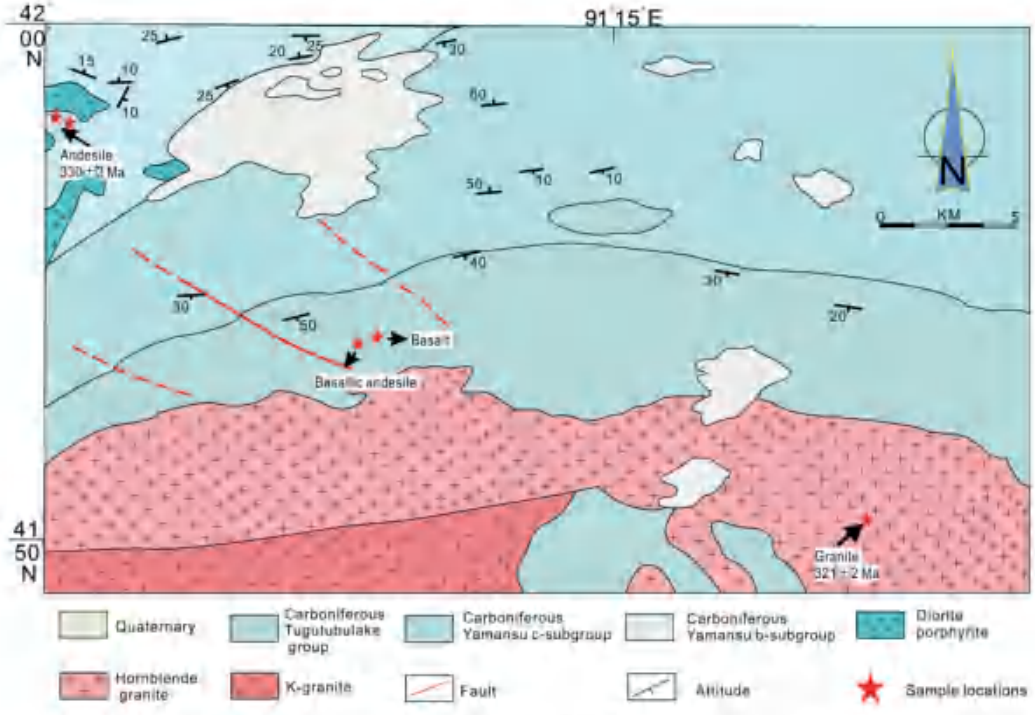

Figure 2. Simplified geological map and sampling sites in the eastern Central Tianshan Block (modified after BGMRXUAR (Bureau of Geology and Mineral Resources of Xinjiang Uygur Autonomous Region) 1993; Long *et al.* 2020).

版权所有(c)国家科技图书文献中心 D2406250153SYJ00

4.1 Zircon U–Pb ages and Lu-Hf isotopic compositions

One sample was selected from each kind of rocks for zircon U-Pb dating and Lu-Hf isotopic analysis. However, two respective samples (16CXS13 and 16CXS44) from the andesite and granite have enough zircons to analyses (Supplementary Table 1 and 2).

Zircons from the andesite (16CXS13) are euhedral to subhedral with 40 ~ 120 μm long with length/width ratios varying from 2:1 to 3:1 (Figure 4(a)). The majority of these zircons are characterized by high Th/U ratios (0.50–1.50), with distinct oscillatory zoning in cathodoluminescence (CL) images. Among the 16 analysed zircons, nine grains yielded $^{206}Pb/^{238}U$ ages between 328 Ma and 332 Ma, which give a weighted mean age of 330 ± 3 Ma (Figure 4(a)). The other seven grains yielded older concordant $^{206}Pb/^{238}U$ ages of 346 Ma, 469 Ma, 493 Ma, 731 Ma, 993 Ma, 1115 Ma and 1334 Ma, indicating these zircons were xenocrysts from the wall-rocks.

Zircons from the granite sample (16CXS44) are mostly stubby, and exhibit component zoning with high Th/U ratios (0.47–0.61), which are similar to the typical

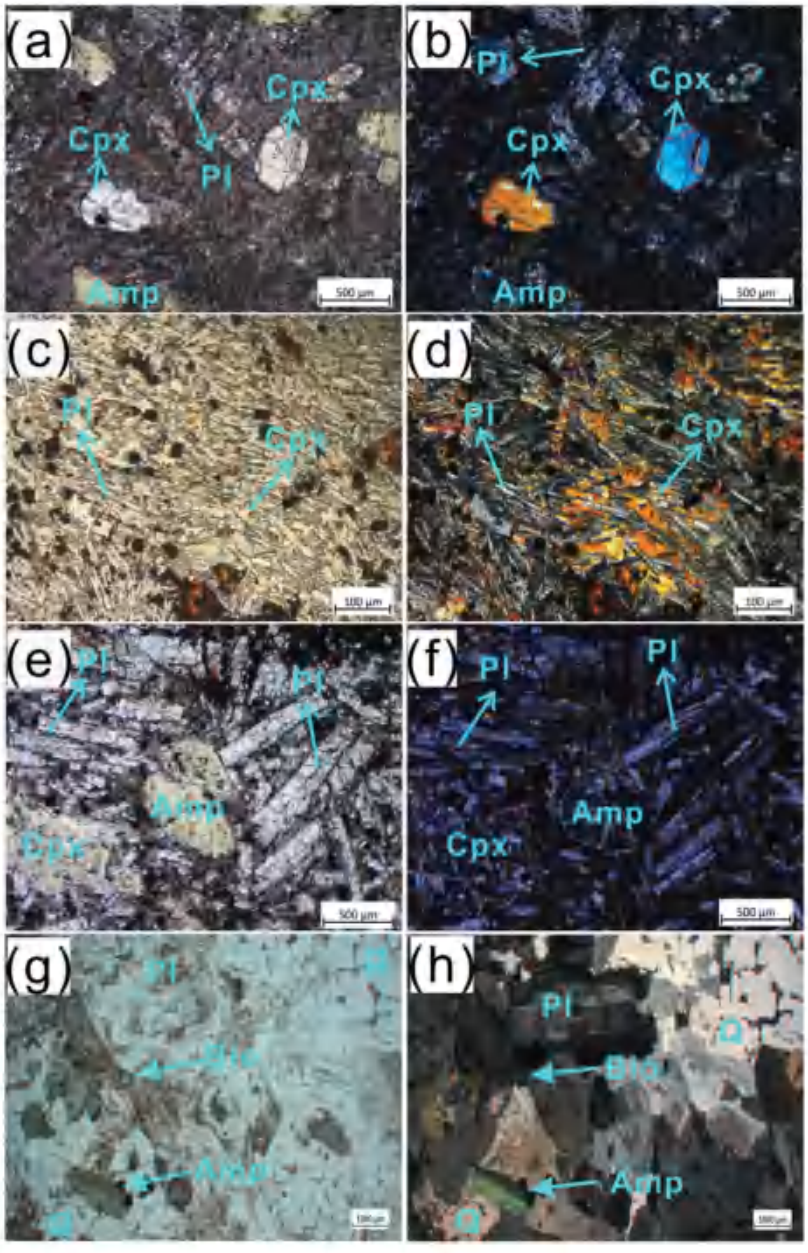

Figure 3. Textural characteristics of the volcanic rocks and intrusive rocks under plane-polarized or cross-polarized light: (a) and (b) basalt, (c) and (d) basaltic andesite, (e) and (f) andesite, (g) and (h) granite. Mineral abbreviations: Amp-amphibole, Q-quartz, Cpx-clinopyxene, Pl-plagioclase.

版权所有(c)国家科技图书文献中心 D240625015355YJ00

magmatic zircons. Size of the zircons ranges from 60 to 150 μm in length with length/width ratios of 1:1 to 3:1. The analyses of 23 grains gave $^{206}Pb/^{238}U$ ages from 310 Ma to 326 Ma, and yielded a weighted mean age of 321 ± 2 Ma (Figure 4(b)). In addition, one older grain yielded a concordant $^{206}Pb/^{238}U$ age of 353 Ma, which is interpreted as inherited zircon from magma source.

In addition, zircons from the andesite and granite were also analysed for in-situ Lu–Hf isotopic compositions by LA–MC–ICP–MS. The ca. 330 Ma magmatic zircon from sample 16CXS13 have relatively low initial $^{176}Hf/^{177}Hf$ ratios (0.282701–0.282792) with variable $\varepsilon_{Hf}(t)$ values (+4.1 to +7.6) (Figure 5(a, b)) and old crustal model ages (T_{DM}^{C}) range from 853 to 1074 Ma. The zircons from sample 16CXS44 show relatively high initial $^{176}Hf/^{177}Hf$ ratios (0.282981–0.283067) with positive $\varepsilon_{Hf}(t)$ values (+14.3 to +17.2) and young T_{DM}^{C} ages (226–425 Ma) (Figure 5(a, b)).

4.2. Whole-rock Sr–Nd isotopes

The whole-rock Sr–Nd isotope analyses of the andesites, basalts, basaltic andesite and granites are listed in Supplementary Table 3 and illustrated in Figure 6. Initial Rb–Sr and Sm–Nd isotopic ratios were calculated based on their zircon U–Pb ages. The basalt and basaltic andesite rocks have initial $^{87}Sr/^{86}Sr$ ratios (I_{Sr}) of 0.703657–0.703851 and 0.705249–0.705444, and $\varepsilon_{Nd}(t)$ values of +5.9 – +6.3 and +1.26 – +1.27, with corresponding young one-stage T_{DM} ages of 0.66–0.71 Ga and 0.95–0.96 Ga, respectively (Figure 6(a); Supplementary Table 3). The andesite rocks have I_{Sr} values of 0.704720–0.705900, with $\varepsilon_{Nd}(t)$ values of −0.02 – +0.62 and one stage T_{DM} ages of 1.40 ~ 1.45 Ga.

4.3. Whole-rock major and trace element compositions

4.3.1. Andesite from the early carboniferous YF

The Yamansu andesites show similar geochemistry characteristics although they displayed two different colours in the outcrops. The andesite samples have variable SiO_2, Al_2O_3, $Fe_2O_3^T$ and Na_2O contents of 58.50–61.37 wt.%, 14.96–15.83 wt.%, 6.81–8.21 wt.% and 2.96–5.92 wt.%, respectively, with uniform and low MgO (3.39–3.65 wt.%), TiO_2 (0.53–0.60 wt.%) and P_2O_5 (0.07–0.08 wt.%) contents (Supplementary Table 4). These samples are mainly plotted into the andesite to trachyandesite fields in the SiO_2 vs. Na_2O+K_2O (TAS) diagram (Figure 7(a)) and the medium-K to high-K and calc-alkaline areas in the SiO_2 vs. K_2O diagram (Figure 7c). In addition, these samples show metaluminous features with A/CNK values of 0.94 to 0.97 (Figure 7(e)).

In the chondrite-normalized rare earth elements (REE) diagram, the andesite samples are characterized by the enrichment of light rare earth elements (LREE) with high $(La/Yb)_N$ ratios (3.04–3.49) and weak negative Eu anomalies (Eu/Eu* = 0.68–0.80) (Figure 8(a)). Besides, these samples show large ion lithophile element (LILE, such as Rb, Ba, Sr, K and Pb) as well as Th and U enrichments, but high field strength element (HFSE, i.e. Nb, Ta and Ti) depletions in the primitive-mantle normalized spider diagram (Figure 8(b)). Moreover, they have moderate Cr (37–79 ppm), Co (19–22 ppm) and Ni (15–19 ppm).

4.3.2. Basalts and basaltic andesite from the late carboniferous TF

The Tugutublak basalts have very uniform SiO_2 (49.36–49.62 wt.%), Al_2O_3 (15.66–15.79 wt.%), $Fe_2O_3^T$ (11.82–11.91 wt.%), MgO (6.46–7.08 wt.%), TiO_2 (1.47–1.52 wt.%), and total alkali ($Na_2O + K_2O$) (3.43–3.60 wt.%). In contrast to those basalts, the basaltic andesite samples

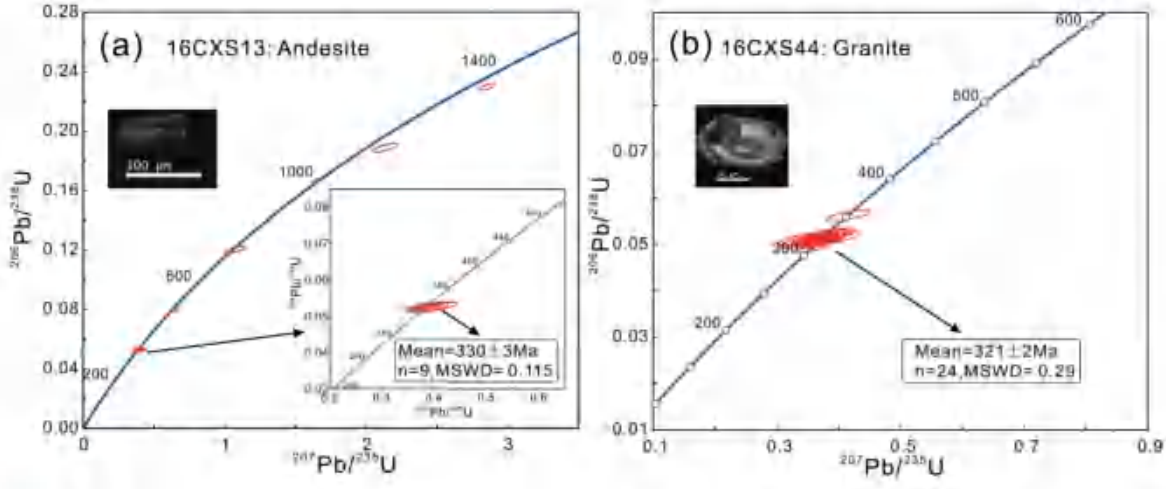

Figure 4. LA-ICPMS zircon U-Pb Concordia diagrams for the (a) andesite and (b) granite.

版权所有(c)国家科技图书文献中心 D240625015355Y100

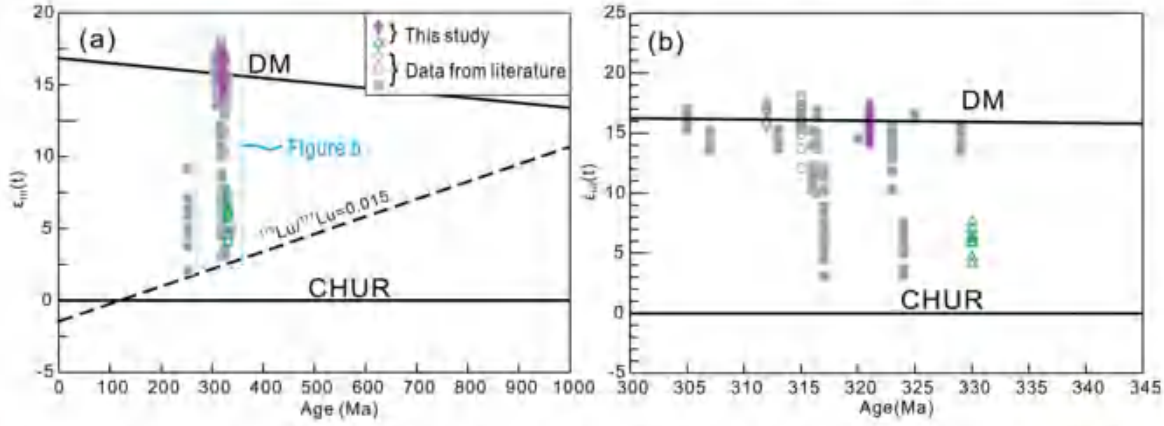

Figure 5. Zircon U-Pb age vs. $\varepsilon_{Hf}(t)$ plots for the felsic rocks in the Aqishan-Yamansu belt. Data are from Zhang *et al.* (2015), Zhang *et al.* (2016), and Zhao et al. (2017, 2018).

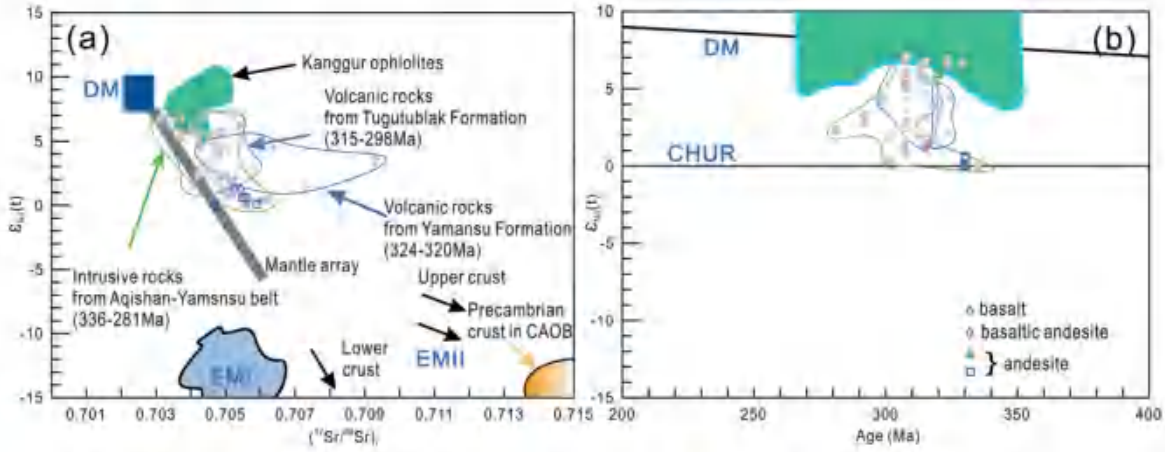

Figure 6. (a) I_{Sr} vs. $\varepsilon_{Nd}(t)$ and (b) age vs. $\varepsilon_{Nd}(t)$ plots for the magmatic rock in the Aqishan-Yamansu belt. Data are from .Yuan *et al.* (2007), Zhou *et al.* (2010), Zhang *et al.* (2013), Hou *et al.* (2014), Luo *et al.* (2016), Jiang *et al.* (2017), Zhang et al. (2016a, Zhang *et al.* 2017), Zhang *et al.* (2017), Du *et al.* (2018a), Zhao *et al.* (2018a), (2018b), and Long *et al.* (2020)

have higher SiO_2 (53.62–54.11 wt.%), Al_2O_3 (16.46–16.73 wt.%) and total alkali ($Na_2O + K_2O$ = 4.86–5.18 wt.%), but lower $Fe_2O_3^T$ (9.10–9.73 wt.%), MgO (3.71–3.93 wt.%) and TiO_2 (~1.18 wt.%). In the TSA diagram, the basalts and basaltic andesites fall into the basalt and basaltic andesite fields, respectively (Figure 7(a)). The basalts have low K_2O contents (0.75–0.87 wt.%), whereas the basaltic andesites have slightly higher contents (K_2O = 1.97–2.10 wt.%), indicating that they are medium-K and high-K calc-alkaline, respectively (Figure 7(c)). Moreover, both the basalts and basaltic andesites in this study have high FeO^T/MgO ratios and show tholeiitic feature in the SiO_2 vs. FeO^T/MgO diagram (Figure 7(d)).

The Tugutublak basalts have relatively high Cr (207–211 ppm) and Ni (111–116 ppm) contents and are characterized by LREE-enriched ($(La/Yb)_N$ = 3.84–3.95) and relatively flat HREE patterns ($(Gd/Yb)_N$ = 1.59–1.65) with weak negative Eu anomalies (Eu/Eu* = 0.96–1.00). In the primitive mantle-normalized diagram, the basalt samples show enrichment of LILEs (i.e. Rb and Ba) and depletion of HFSE (i.e. Nb, Ta and Ti) (Figure 8(c, d)). In contrast, the basaltic andesites have lower Cr (133–168 ppm), Ni (50–57 ppm) and Co (24.8–26.9 ppm), and remarkably LREE enrichment features ($(La/Yb)_N$ = 11.7–12.6) and moderate HREE fractionation ($(Gd/Yb)_N$ = 2.26–2.42), with slightly negative Eu anomalies (Eu/Eu* = 0.91–0.97) (Figure 8(e)). In the primitive mantle-normalized diagram (Figure 8(f)), the Tugutublak basaltic andesites show very similar patterns to the basalts but with higher LILE concentrations.

4.3.3. Late Carboniferous Bailingshan granite

The Bailingshan granite samples have high SiO_2 (69.2–70.1 wt.%) and total alkali contents ($K_2O + Na_2O$ = 6.67–7.01 wt.%), but low $Fe_2O_3^T$ (3.49–3.97 wt.%), MgO (0.99–1.09 wt.%) and TiO_2 (0.34 ~ 0.39 wt.%) contents. They are plotted in the granite field in the TAS diagram (Figure 7

版权所有(c)国家科技图书文献中心 D240625015355Y00

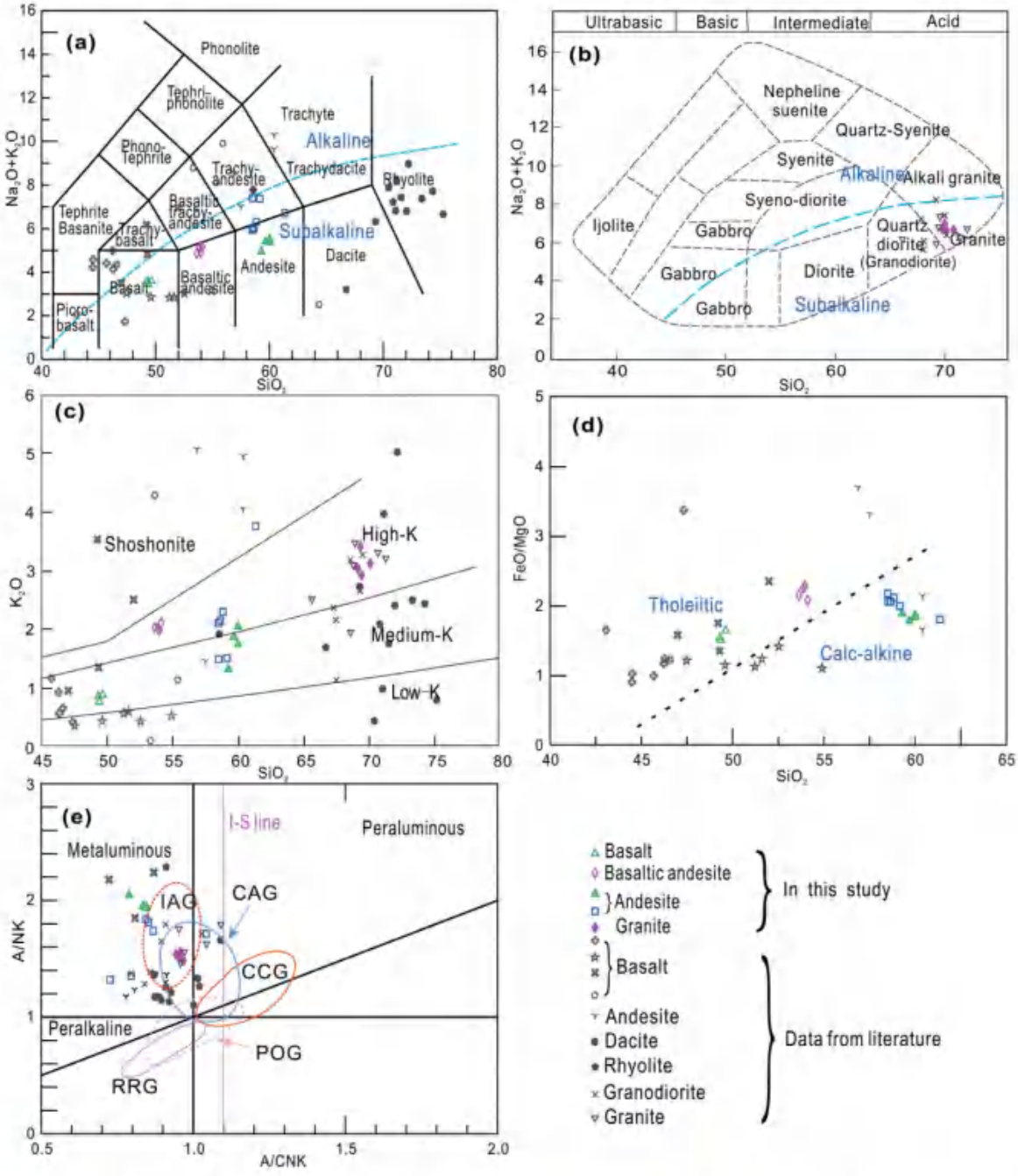

Figure 7. (a) Total alkali-silica (TAS) diagram for volcanic rocks (after Middlemost 1994); (b) TAS classification diagram for intrusive rocks, the alkaline and sub-alkaline division is after irvine and Baragar (1971); (c) SiO_2 vs. K_2O plot for the volcanic rocks (after Peccerillo and Taylor 1976); (d) FeO^T/MgO versus SiO_2 plot to distinguish tholeiitic and calc–alkaline magma series (after Miyashiro 1974); (e) A/CNK vs. A/NK plot (after Maniar and Piccoli 1989). Literature data for coeval magmatic rocks in the Aqishan-Yamansu belt (Zhang *et al.* 2013, 2016; Jiang *et al.* 2017; Zhao et al., 2017). Abbreviation: IAG, Island Arc Granites; CAG, Continental Arc Granites; CCG, Continental Collision Granites; POG, Post-orogenic Granites; RRG, Rift-related Granites.

(b)). The granites have high K_2O contents (2.92–3.41 wt. %) and show high-K calc-alkaline features in the SiO_2 vs. K_2O diagrams (Figure 7(c)). Similar to the andesites, the granites have moderate A/CNK ratios (0.91–0.97), indicating metaluminous characteristics (Figure 7(e)).

In the chondrite-normalized REE diagram, the Bailingshan granites have uniform REE patterns and are characterized by enrichment of LREEs ($(La/Yb)_N$ = 2.50–5.74), with negative Eu anomalies (Eu/Eu* = 0.58–0.84) (Figure 8(g)). Similar to the above

版权所有(c)国家科技图书文献中心 D2406250153SYJ00

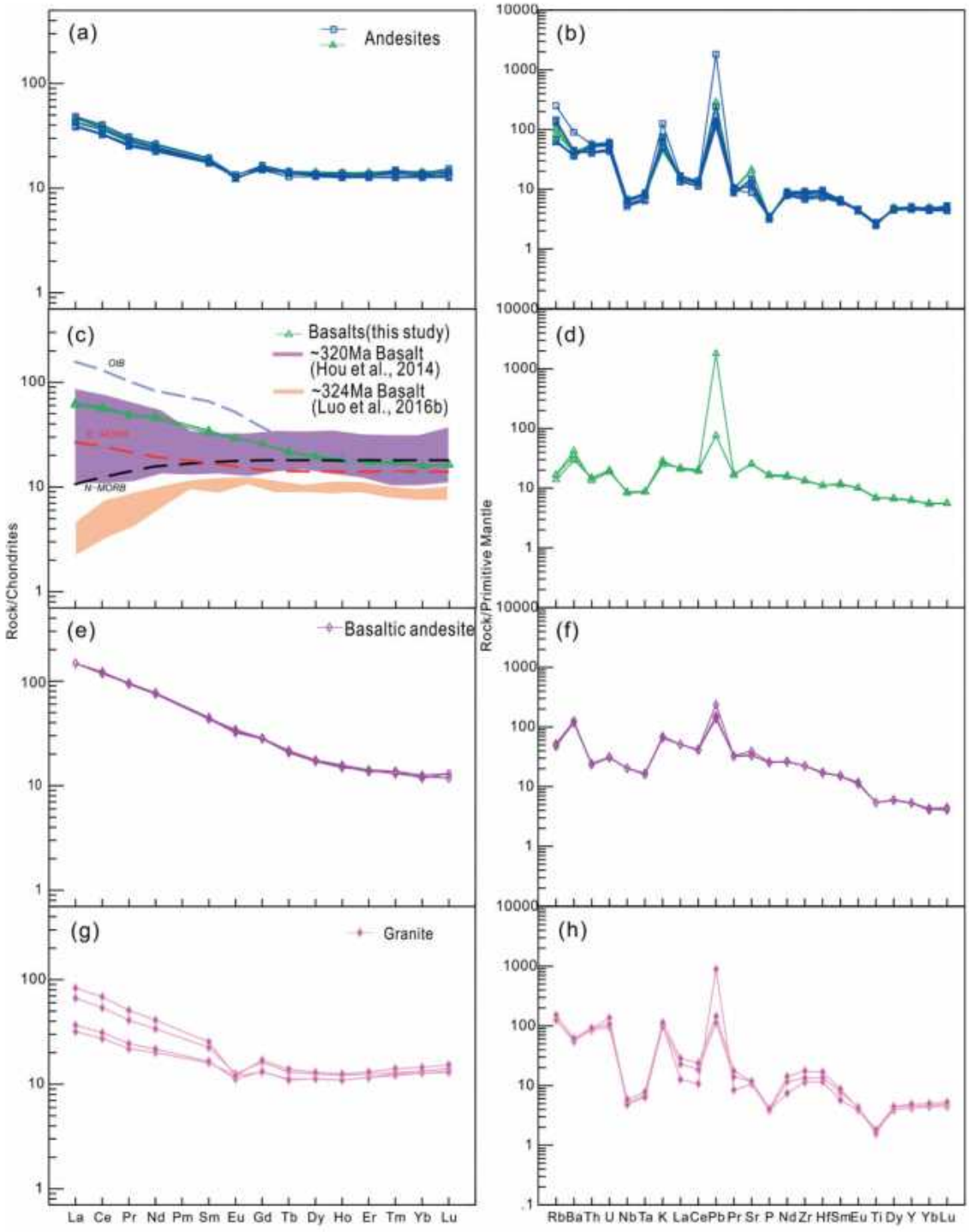

Figure 8. Chondrite-normalized REE patterns and primitive mantle-normalized multi-element diagrams for the (a-b) basalt, the (c-d) andesite, the (e-f) basaltic andesite, and the (g-h) granite. Normalizing values are from Sun and McDonough (1989). Abbreviation: OIB, curve of Ocean Island Basalt; E-MORB, curve of E-type Mid-Ocean-Ridge Basalt; N-MORB, curve of N-type Mid-Ocean-Ridge Basalt.

版权所有(c)国家科技图书文献中心 D240625015355YJ00

andesite, these granites also enriched in LILEs as well as Th and U, and depleted in HFSEs (Figure 8(h)), but have lower Cr (26.4–27.4 ppm), Co (1.01–1.22 ppm) and Ni (0.40–1.05 ppm).

5. Discussion

5.1. Age of the YF and the TF

The YF and the TF are both distributed in east–west direction and controlled by the Aqikuduke and Yamansu faults. Recently, Su *et al.* (2009) obtained a zircon SHRIMP U–Pb age of 341.7 ± 2.7 Ma for the dacite in the YF. Then, Luo *et al.* (2012) reported three LA-ICP-MS U–Pb zircon ages for the YF, including an age of 348 ± 2 Ma in the eastern section, 336 ± 2 Ma in the middle, and 334 ± 3 Ma in the western section. Hou *et al.* (2014) reported a LA-ICP-MS zircon U–Pb age (324 ± 1 Ma) for the Yamansu basalt and basaltic andesite. In this study, we obtain the weighted average age of 330 ± 3 Ma for the andesite in the YF. These age data show that the YF was formed at Early Carboniferous.

Rocks of the TF were exposed on both sides of the Aqikekuduke fault (Zhang et al., 2012b). Zhang *et al.* (2016) reported the LA-ICP-MS zircon U–Pb age of 324 ± 2.1 Ma for the Bailingshan tuffaceous dacite. Meanwhile, Luo *et al.* (2016) reported LA-ICP-MS U–Pb dating results of basalt (ca. 320 Ma) and basaltic andesite (ca. 321 Ma) from the TF, respectively. Therefore, the ca.320 Ma which cited here can approximately represent the age of basalt and basaltic andesite in this study. In this study, the newly-obtained zircon U–Pb age of the Bailingshan granite is ca. 321 Ma. Integrate with the previously published data, we suggest that the volcanism of the TF had been active till ~320 Ma, and the studied basalt and basaltic andesite in the TF were formed between ~320–324 Ma.

5.2. Petrogenesis and magma source

5.2.1. Andesites from the Early Carboniferous YF

In this study, the Yamansu andesites show subalkaline and calc-alkaline characteristics with moderate SiO_2 (58.5–61.4 wt.%), but higher $Mg^{\#}$ (49–54) than the experimental melts from metabasalt and eclogites (Supplementary Table 4, Figure 7 (a–Figure d); Figure 9 (a)), suggesting that mantle melting plays a significant role rather than crustal melting. Melting of mantle source will produce the residuum with high Zr/Nb ratio, owing to Nb is more incompatible element than Zr. The studied andesites possess higher Zr/Nb ratios (20.3–21.9) than that of the primitive mantle (Zr/Nb = 15.7; Sun and McDonough 1989), indicative of a depleted mantle source. This is also supported by the depletion of HSFE (Figure 8(b)) and low Nb/Ta ratios (12.3–14.5) (Supplementary Table 1), which are closed to those of depleted mantle 15.47 (Rhea and Stanley 2005). However, these Early Carboniferous andesites have pronounced negative Nb, Ta and Ti anomalies, which are different from N-MORB and OIB (Sun and McDonough 1989). Moreover, their Zr/Nb ratios (20.3–21.9) are lower than those of N-MORB (31.8) (Sun and McDonough 1989), suggesting they cannot be originated from the depleted asthenosphere mantle directly (Su *et al.* 2012). Generally, there are four petrogenesis models for andesites, i.e. crystallization differentiation of basic magma (Langmuir 1989), partial melting of basaltic rocks (such as subduction oceanic crust) (Petford and Gallagher 2001), mixing of basic and acid magma (Downes *et al.* 1990; Griffin *et al.* 2002), and partial melting of metasomatic mantle (Richards and Kerrich 2007). The andesite formed by crystallization differentiation of basic magma is usually accompanied with coeval basalts spatially and is expected to exhibit obvious negative Eu anomalies (Peccerillo *et al.* 2003). However, there is no Early Carboniferous basalts exposed around our samples, and the andesites in this study show slight negative Eu and Sr anomalies. Thus, the petrogenesis of crystallization differentiation can be excluded. The andesites in this study show a partial melting trend rather than fraction crystallization in La vs. La/Sm diagram (Figure 10d). The low $\varepsilon_{Hf}(t)$ values (+4.1 to +7.6) and Na_2O/K_2O (mostly 0.80–2.77) ratios of these andesites are distinct to those andesites generated by partial melting of subduction oceanic crust (Zhu *et al.* 2009). For andesites formed by the mixing of basic and acidic magma, mafic microgranular enclaves or disequilibrium structures, such as forsterite, variable composition of plagioclase porphyry, and the core with melting structure will coexist in the rocks. The above evidences were not found in the andesites of this study, so magma mixing could also be excluded for the investigated andesites. The Yamansu andesites show pronounced depletion of HFSE (e.g. Nb, Ta, and Ti) and enrichment in LILEs (e.g. Rb, K and Pb) (Figure 8b), indicating a geochemical feature of typical subduction-related magmas (Mcculloch and Gamble 1991). Firstly, the narrow range of SiO_2 (58.5 wt.% ~61.37 wt.%) and $\varepsilon_{Nd}(t)$ (−0.02 to +0.62) do not indicate crustal contamination. In addition, crustal contamination-sensitive trace elements or element ratios (e.g. Th, Zr, Nb/La, $(La/Sm)_N$) of the andesite in this study not correlated with MgO, inconstant with contamination (Wang *et al.* 2013). The Th and Nb elements have different mobility in the fluids, thus they will change after crustal contamination and subducted-material influence. According to this, the Th/Yb vs. Nb/Yb diagram is

版权所有(c)国家科技图书文献中心 D240625015351Y100

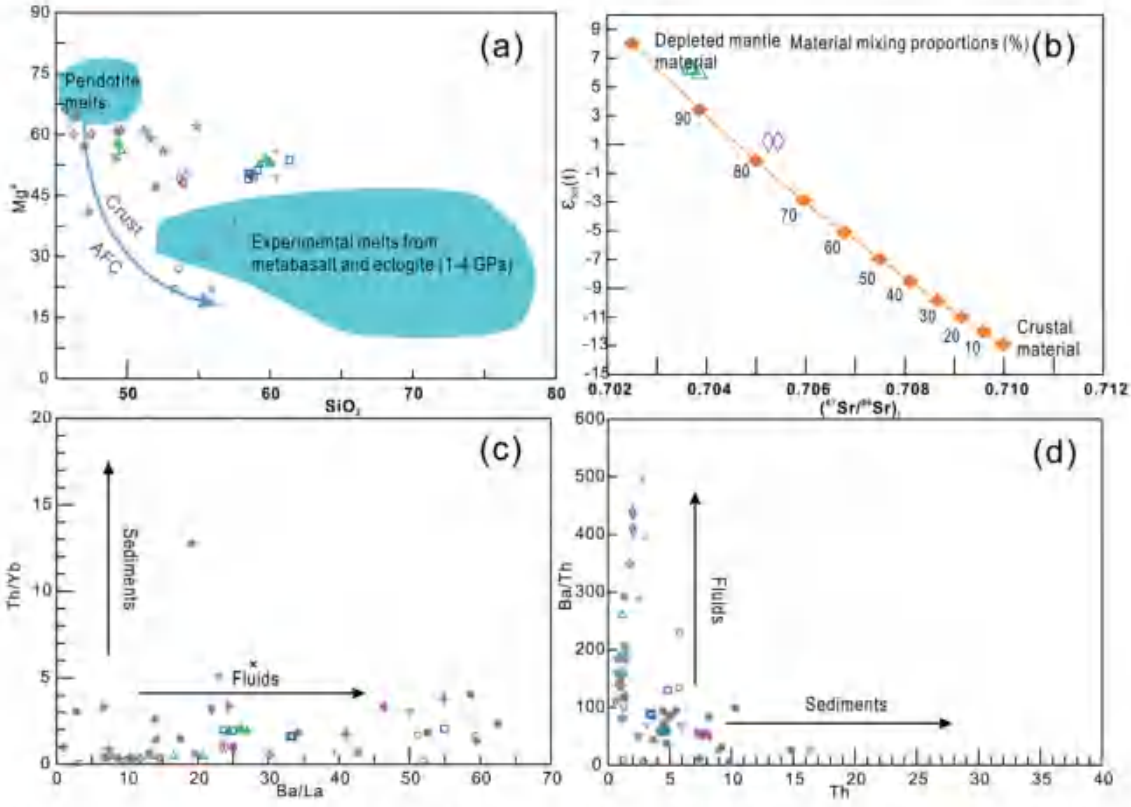

Figure 9. (a) SiO_2 vs. $Mg^{\#}$ plot, supposed peridotite melts and crust AFC curve are after Stern and Kilian (1996). The field for metabasalt and eclogite experimental melts (1–4.0 GPa) are from Rapp *et al.* (1999, and references therein). (b) $\varepsilon_{Nd}(t)$ vs. $(^{87}Sr/^{86}Sr)_i$ plot, showing source mixing proportions between two end-members. Depleted mantle (represent juvenile components): Sr = 150 ppm, $(^{87}Sr/^{86}Sr)_i = 0.7025$, Nd = 15 ppm, $\varepsilon_{Nd}(t) = +8$ (from Jahn *et al.*). Mesoproterozoic crust basement: Sr = 300 ppm, $(^{87}Sr/^{86}Sr)_i = 0.710$, Nd = 38 ppm, $\varepsilon_{Nd}(t) = -13$ (from Hu *et al.* 2000). (c) Ba/La vs. Th/Yb plot (after Woodhead *et al.* 2001). (d) Th vs. Ba/Th plot (after Hawkesworth *et al.* 1997).

able to reveal the input of crustal or subduction-related materials into the magmas (Pearce 2008). All of our andesite samples plotted above the mantle array and near the subduction component input field, but far from the area of crustal contamination (Figure 10a) (Li et al., 2013). Consequently, we conclude that the andesite magma might have originated from a subduction-related source without obvious crustal contamination.

Subduction-related materials generally contain hydrous melts and slab-derived fluids. During the process of subduction, it is generally accepted that the fluids enriched in LILE from the subducting slab are released and ascent into the overlying mantle wedge (Hawkesworth *et al.* 1997; Woodhead *et al.* 2001). High Rb/Y (1.82–4.23) and Ba/La (23.6–54.9), low and constant Nb/Y (0.18–0.21) and Th/Yb (0.37–0.43) ratios (Figure 9c), combined with enrichment of LREE and notable depletion of HSFE in the andesite of this study strongly suggest that the magma source was probably affected by slab-derived hydrous fluids (Woodhead *et al.* 2001). Subducted sediment-derived melts have high Th, low Ba and Ce, and relatively low Ce/Th (~8) and Ba/Th (~111) (Plank and Langmuir 1998), and high Th/Ta ratios (Pearce *et al.* 2005). Therefore, the high Th (3.39–4.82 ppm) and relatively low Ce/Th (5.04–5.85) and Ba/Th (almost between 57.2 and 89.4, one 129.8) ratios of the andesites (Figure 9d) suggest a contribution from subducted sediment-derived melts in the magma source. Therefore, the andesites were suggested to be produced by partial melting of a depleted mantle wedge metasomatized by both subducted sediment-derived melts and slab-derived aqueous fluids.

5.2.2. Basalts and basaltic andesites from the Late Carboniferous TF

The Tugutublak basalts display typical tholeiitic characteristics with relatively low SiO_2 (49.36–49.62 wt.%), high MgO (6.46–7.08 wt.%) and $Mg^{\#}$ (56–58), and relatively high contents of compatible trace elements, such as high Cr (207–211 ppm), Ni (111–116 ppm), and Co (40–42 ppm), indicating mantle component played an important role in their genesis (Tang *et al.* 2014; Wang *et al.* 2016a). The rocks also have lower $(La/Sm)_{PM}$ ratios

版权所有(c)国家科技图书文献中心 D240625015355Y100

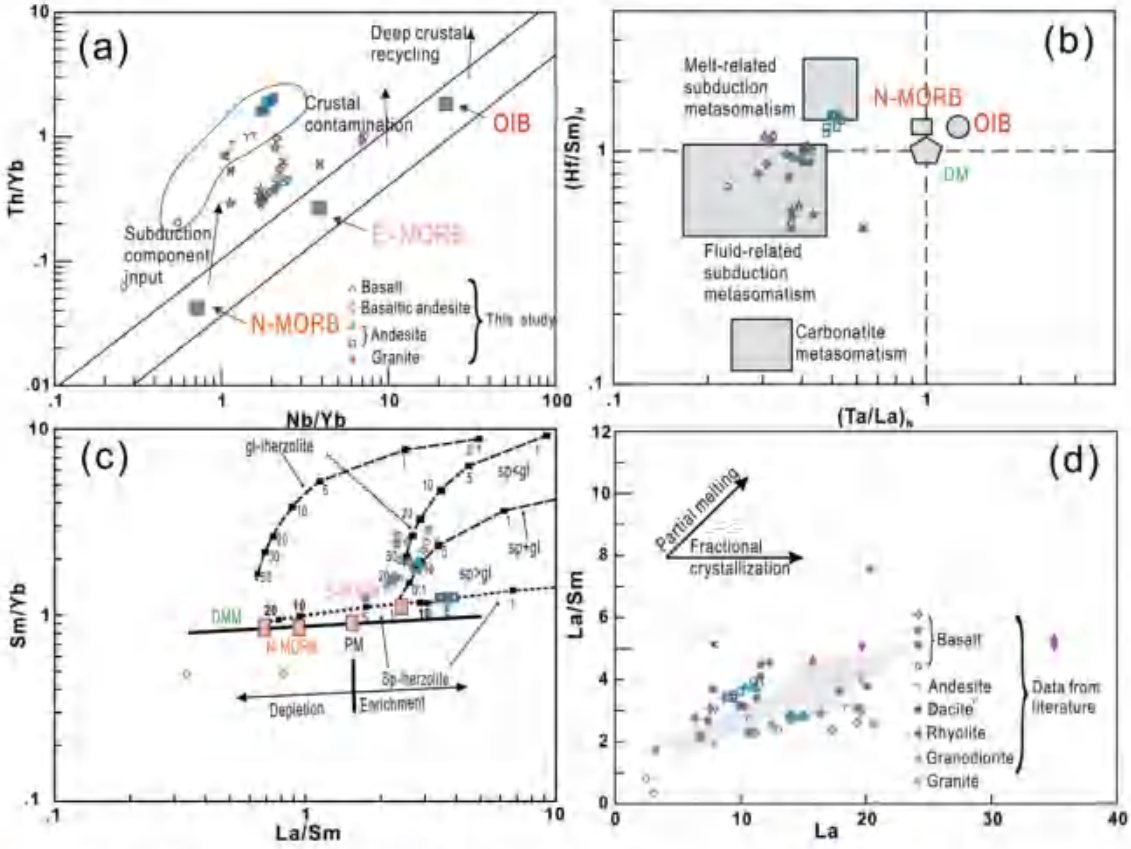

Figure 10. (a) Nb/Yb vs. Th/Yb plot (after Pearce 2008), Mariana IAB are from Pearce *et al.* (2005); (b) $(Ta/La)_N$ vs. $(Hf/Sm)_N$ plot (after LaFlèche *et al.* 1998). (c) La/Sm vs. Sm/Yb plot (after Aldanmaz *et al.* 2000). (d) La vs. La/Sm plot.

(1.81–1.83) than those of OIB-like magmas ($(La/Sm)_{PM} \gg 1$; Niu 2010), which suggest our samples could not be derived from an OIB source. Besides, the depletions in Nb-Ta-Ti are different from OIB (Figure 8c, d). Primary basaltic magmas originated from partial melting of mantle peridotite commonly have high $Mg^{\#}$ (68–75) (Hanson and Langmuir 1978), Ni (250–300 ppm), Cr (500–600 ppm) and Co (27–80 ppm) (Wilkinson and Le Maitre 1987). In contrast, our basalt samples have lower Ni (111–116 ppm), Cr (207–211 ppm) and $Mg^{\#}$ (56–58) than primary basaltic magma, suggesting a derivation from relatively evolved melts rather than a primary mantle-derived magmatic source. Moreover, the basalts in this study show enrichment of LREE, enriched in LILE but depleted in HFSE (e.g. Nb, Ta, and Ti) (Figure 8d), without Eu anomalies on the chondrite–normalized diagram (Figure 8c). All of those characteristics reflect subduction signatures or crustal contamination (Rudnick and Gao 2003). The uniform range of SiO_2 (49.36–49.62 wt.%) and $\varepsilon_{Nd}(t)$ (+5.9 to +6.3), and no significant Zr–Hf positive anomalies suggest that the basalts were not influenced by significant crustal contamination. Therefore, the formation of the Tugutublak basalts was most likely derived from melts influenced by subducted-related materials.

Slab-derived fluids generally transport water-soluble elements, but hydrous melts can transport both water-soluble and water-insoluble elements (Zheng 2012). The partial melting of mantle metasomatized by slab-derived fluid would produce magmas with high Ba/Th ratios (Pearce *et al.* 2005). However, partial melting of mantle influenced by slab-derived melts may give rise to high Th/Ta ratios (Pearce *et al.* 2005). The high Ba/Th (161–260) (Figure 9d), slight low Th/Ta (3.14–3.62) ratios and high contents of highly mobile elements (e.g. Rb, Cs, Ba, U and Pb) (Figure 8d) of the Tugutublak basalts indicate the influence of slab-derived fluids. Besides, their high Rb/Y (0.31–0.38) and Ba/La (13.5–24.7), but low and constant Nb/Y (0.21–0.22) and Th/Yb (0.43–0.46) ratios (Figure 9c) also suggest that the subduction materials were most likely dominated by slab-derived fluids (Woodhead *et al.* 2001). Additionally, all the basalt samples were plotted in the area of fluid-related subduction metasomatism in $(Th/La)_N$ vs. $(Hf/Sm)_N$ diagram (Figure 10b). Meanwhile, the basalts have relatively high $\varepsilon_{Nd}(t)$ values (5.9–6.3) and low initial $^{87}Sr/^{86}Sr$ ratios (0.703657–0.703851), and plotted into the area of Kanggur ophiolites (Figure 6), suggesting that it was derived from depleted mantle. The trace elements and the Sr-Nd

版权所有(c)国家科技图书文献中心 D2406250153SYJ00

isotopes characteristics reveal that the mantle source was metasomatized by slab-derived hydrous fluids before generating the Tugutublak basalts.

Lithospheric thickness can be modelled using the related trace elements or elements ratios (Aldanmaz *et al.* 2000). High partition coefficient for Yb ($D_{garnet/melt}$ = 6.6) relative to Sm ($D_{garnet/melt}$ = 0.25) results in strong change of Sm/Yb ratio in various degree partial melting of garnet lherzolite mantle with residual garnet (Green 2006). Spinel has similar partition coefficients for Sm and Yb (Aldanmaz *et al.* 2000). Therefore, the Sm/Yb ratios do not change when the spinel lherzolite mantle partially melt. Consequently, the Sm/Yb ratio can be used to distinguish the melts of garnet lherzolite mantle from spinel lherzolite mantle. The basalts of this study show increasing La/Sm ratios at nearly constant Sm/Yb ratios in a La/Sm versus Sm/Yb diagram (Figure 10c), which suggests that the basalts were derived from partial melting of a spinel-facies lherzolite mantle and a relatively shallow depth of melting (<80 km).

The basaltic andesites show similar REE patterns and trace element patterns to the Tugutublak basalts in the primitive mantle-normalized diagram (Figure 8c-f), but have lower $Mg^{\#}$ (48–50), Cr (133–168) and Ni (50–57). We suggest that the basaltic andesites were evolved from the basaltic melts after limited fractional crystallization of mafic minerals. In addition, the lower $\varepsilon_{Nd}(t)$ and higher $(^{87}Sr/^{86}Sr)_i$ values of the basaltic andesite may suggest a more significant involvement of crustal materials in their genesis. The basaltic andesites in this study show slightly positive Zr–Hf anomalies in the chondrite-normalized REE patterns, indicative of crustal material contamination (Figure 8f). To better assess the genetic relationship between basaltic andesite and basalt from the TF, a simple mixing model using different end-members is show in Figure 9b. The depleted juvenile end-member is presented by mantle-derived basaltic rocks from the Kangguer ophiolites and the old end-member is presented by Precambrian crustal basement rocks. According to the simulation, the Tugutublak basaltic andesite can be derived from the Tugutublak basalt magma with an input of crustal material (~20%). Therefore, the basaltic andesite in this study were most likely derived from a same mantle source with the Tugutublak basalt, but experienced obvious crystallization of mafic minerals with more crustal material involved.

5.2.3. Late Carboniferous Bailingshan granite

Granitic rocks can be subdivided into three types (I-, S-, and A-types) according to their chemical compositions (Bonin 2007). The Bailingshan granites in this study are metaluminous with A/CNK values ranging from 0.94 to 0.97, and have low P_2O_5 (0.05–0.09 wt.%) and high Na_2O (3.57–3.81 wt.%), different from S-type granites that generally are peraluminous with A/CNK >1.1 and have high P_2O_5 and low Na_2O (Zhao et al., 2018a), but show geochemical features of I-type granites in the diagram of SiO_2 vs. P_2O_5 (Figure 11a). Besides, the absence of typical Al-rich minerals (cordierite and garnet) in the samples further excludes an origin of S-type granite. The granites are identified as calc-alkaline series (Figure 7b, d) with low Zr and Ce contents (129–197 ppm and 17–42 ppm) and 10,000*Ga/Al ratios (1.64–1.83), clearly distinct from typical A-type granites (Figure 11b, Collins *et al.* 1982; Whalen *et al.* 1987). Therefore, the Bailingshan granites belong to I-type granites.

The Bailingshan granites are characterized by low MgO (0.99–1.09 wt.%), CaO (2.80–3.26 wt.%) and $Fe_2O_3^T$ (3.49–3.97 wt.%) contents, strongly enrichment of LILEs and depletion in HFSEs (Figure 8g, h). All of those are typical features of subduction-related magmatic rocks (Mcculloch and Gamble 1991). Highly positive and homogeneous $\varepsilon_{Hf}(t)$ values (+14 ~ +17) of magmatic-type zircons, as well as the presence of inherited zircons (an inherited grain with an age of 352 Ma), suggest significant contribution from juvenile materials with minor involvement of old crustal components during magma formation.

5.3. Formation of the Aqishan–Yamansu Belt

In recent two decades, the evolution process of the Aqishan–Yamansu Belt became much clear (Xiao *et al.* 2004, 2013; Wu *et al.* 2006; Zhou *et al.* 2010; Lei *et al.* 2013; Zhang *et al.* 2013; Hou *et al.* 2014; Zheng 2015; Luo *et al.* 2012, 2016; Zhang *et al.* 2016, Zhao et al., 2017; Zhao *et al.* 2018b; Du *et al.* 2018a, 2018b). There is a consensus that the formation of this belt is related to subduction process, which is evidenced by a large number of arc-related volcanic rocks and intrusive rocks (Wu *et al.* 2006; Zhou *et al.* 2010; Lei *et al.* 2013; Zhang *et al.* 2013; Hou *et al.* 2014; Zheng 2015; Luo *et al.* 2012, 2016; Zhang *et al.* 2016, Zhao et al., 2017; Zhao *et al.* 2018b; Du *et al.* 2018a, b). Nevertheless, the issues with regard to subduction oceanic slab, subduction polarity in this belt are still debatable. Xiao *et al.* (2004) and Han *et al.* (2014) proposed that the Aqishan–Yamansu Belt was formed by northward subduction of South Tianshan oceanic slab, but Li *et al.* (2011), Hou *et al.* (2014) and Zhang *et al.* (2016) argued that this belt as product of southward subduction of Junggar oceanic slab. Alternatively, Wang *et al.* (2015) considered that the Aqishan–Yamansu Belt was formed by the northward subduction of the Kanggur oceanic slab.

版权所有(c)国家科技图书文献中心 D2406250153SY00

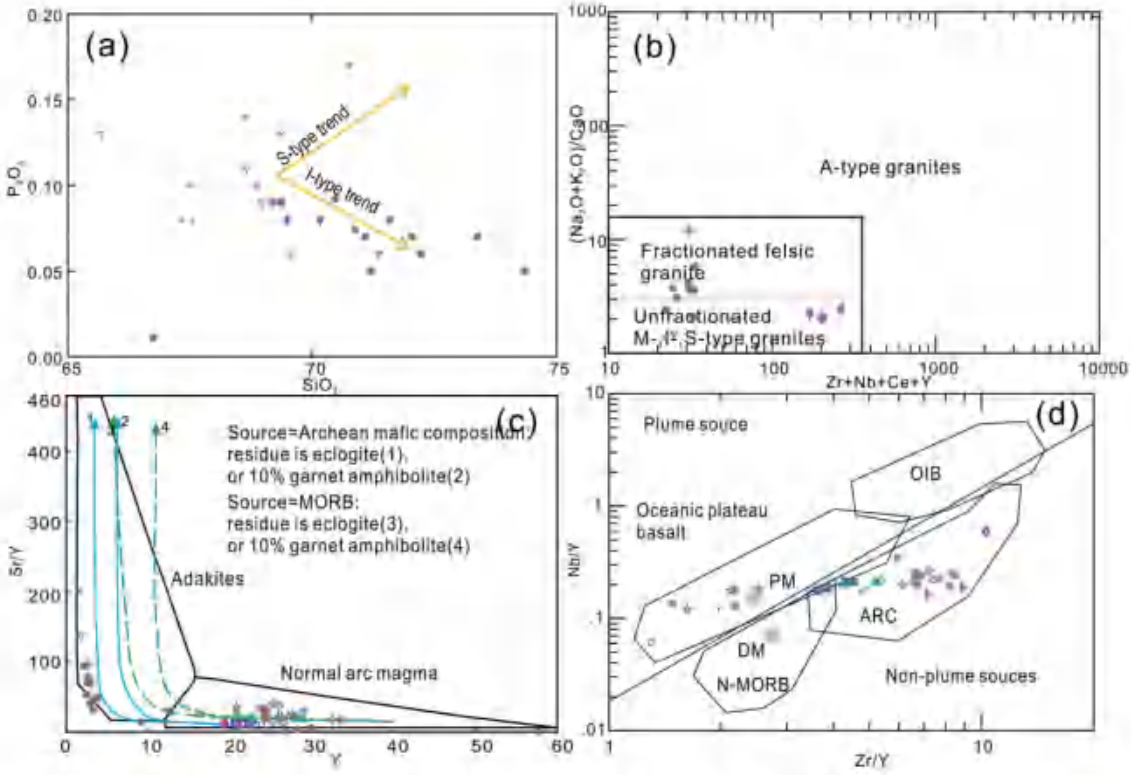

Figure 11. (a) SiO_2 vs. P_2O_5 plot (after Peccerillo and Taylor 1976); (b) (Zr+Nb+Ce+Y) vs. $(K_2O+Na_2O)/CaO$ plot (after Whalen *et al.* 1987); (c). Y vs. Sr/Y plot. Fields for adakites and classical island arc magmatic rocks are from Defant and Drummond (1990); (d). Zr/Y vs. Nb/Y plot for the basaltic rocks (after Condie 2005).

The geochemistry of the volcanic rocks in this study, together with the published data, suggests that the Aqishan–Yamansu Belt was formed by the southern subduction of the Kanggur ocean plate. This is supported by the following evidence. (1) the age of the Kanggur ophiolite along the Kanggur fault manifest that the Kanggur ocean plate was really existed prior to 494 Ma (Li *et al.* 2000, 2008). (2) The Precambrian inherited zircons from the Yamansu felsic volcanic rocks show similar age peaks to those from the basement rocks of the CTB (ca. 900 Ma and 1400 Ma) (Luo *et al.* 2012). These Precambrian inherited zircons have old crustal model ages (T_{DM}^{C} = 853–1074 Ma), which indicate that the arc was built on the Precambrian basement of the Central Tianshan Block. (3) The underlying YF occurred in the northern part of the Aqishan–Yamansu belt whereas the overlying TF was exposed in the southern part. The spatial and temporal distributions of volcanic rocks are consistent with the younger trend away from the ocean trench in an active continental margin (Villagómez *et al.* 2011). Therefore, we suggest that the Aqishan–Yamansu Belt was formed by the southward subduction of the Kanggur oceanic slab beneath the CTB.

5.4. The Carboniferous variation of slab angles in the Aqishan–Yamansu Belt

It is commonly approved that arc and basin system represent two respective states of compression and extension, since slab/trench advance and retreat commonly resulted in crustal thickening and thinning, respectively (Zhang *et al.* 2018). Because crustal thickness determines the length of magma passing through the crust, the probability of crystal differentiation, and the degree of crustal contamination during its ascent, the variation of crustal thickness can provide important information for the subduction–accretion process (Mamani *et al.* 2010; Zhang *et al.* 2018). The thickening of the crust will cause the lower part of crust in a high-pressure state, resulting in the high-pressure minerals (e.g. garnet) developed into a stable phase (Mamani *et al.* 2010). Therefore, some geochemical ratios have been used to estimate crustal thickness, such as Ce/Y ratios for basalt–basaltic rocks, Sm/Yb, Sr/Y, La/Yb, La/Sm, Dy/Yb, and Ho/Yb ratios for crust–derived felsic rocks. These element ratios are related to the absence or presence of plagioclase (or garnet) in magma genesis (Mamani *et al.* 2010; Chapman *et al.* 2015). Based on the distribution

版权所有(c)国家科技图书文献中心 D2406250153SYJ00

felsic rocks in the Aqishan–Yamensu belt, we chose Ho/Yb and Dy/Yb ratios of felsic rocks (SiO_2 > 56 wt.%) to infer the variation of crustal thickness during the Carboniferous. The elements of Ho, Dy and Yb, as HREE, prefer distributing into amphibole and garnet during partial melting and magmatic differentiation. However, the partition coefficients (D_{Ho}/D_{Yb}, D_{Dy}/D_{Yb}) between garnet and melts are uniform than that between amphibole and melts (e.g. Shuto *et al.* 2013). Thus, the Ho/Yb and Dy/Yb ratios of felsic melts are closely related with garnet rather than amphibole. More important, the garnet and amphibole have different preferences for Ho, Dy and Yb, with the increase of SiO_2, and the Ho/Yb and Dy/Yb ratios significantly increase with garnet fractionation and slightly decrease with amphibole fractionation (Dessimoz *et al.* 2012). Therefore, the Ho/Yb ratio of felsic magma without garnet fractionation can be used as the indicative of residual garnet, that is, the maximum Ho/Yb and Dy/Yb ratio can constrain the minimum melting depth and crustal thickness.

The felsic rocks (SiO_2 > 56 wt.%) in the Aqishan–Yamansu Belt do not exhibit obvious correlations of Ho/Yb and Dy/Yb with SiO_2, arguing against significant crystallization effect on the variable Ho/Yb and Dy/Yb ratios. The Ho/Yb and Dy/Yb ratios could therefore provide constraints on the variation of crustal thickness in the Aqishan–Yamansu Belt (Figure 12). On the basis of the collected data, four periods of crustal thickness changing can be distinguished in the Aqishan–Yamansu Belt (Figure 12): (1) crustal thickening in the middle Mississippian; (2) crustal thinning in the late Mississippian; (3) crustal thickening in the early Pennsylvanian; (4) crustal thinning in the middle to late Pennsylvanian.

Phase 1: the Ho/Yb and Dy/Yb ratios gradually increased before ~330 Ma, indicating the crustal thickened. As mentioned above, thickening of the crust thickness is associated with slab advance, which means a continuous subduction. This is also consistent with the arc-related rocks occurred during this period in the Aqishan–Yamansu Belt. The earliest volcanic rocks are the Yamansu basaltic andesites and the earliest intrusive rocks are the Xifengshan granites, which yielded coeval zircon U–Pb ages of 348 ± 2 and 349 ± 3 Ma, respectively (Zhou *et al.* 2010; Luo *et al.* 2012, 2016). Wang *et al.* (2016a) reported that the ages of the syenogranites and alkali feldspar granites from the Hongshi gold deposit are 338 Ma and 334 Ma, respectively. Du *et al.* (2018a) revealed that the ages of arc-related granodiorite and dioritic enclaves in Aqishan–Yamansu Belt are 336 Ma and 335 Ma, respectively. All above magmatic rocks are enriched in LREE and LILE (e.g. Rb, K, Ba, and Pb), but depleted in HFSE (e.g. Nb, Ta, P, and Ti), indicating an arc tectonic setting. These arc-related rocks and their ages may represent the initial subduction happened no later than 350 Ma. In this study, the 330 ± 3 Ma andesites show calc-alkaline affinities with LREE and LILE enrichment and HFSE depletion (e.g. Nb, Ta, P, and Ti), exhibiting characteristics of arc-related magmatic rocks (Rollinson 1993). They plot in the field of VAG and normal arc magma in the diagrams of Rb vs. Y+ Nb, Y vs. Sr/Y and Th-3/Hf-Ta (Figures 10 c-d and 13a-b). Therefore, arc-related magmatic activity in the Aqishan–Yamansu Belt was at least ongoing between 350 Ma to 330 Ma, and the region was in a state of compression during that time. This period is linked with the initial southern subduction of the Kanggur ocean slab, compatible with the formation of the Early Carboniferous arc-related rocks.

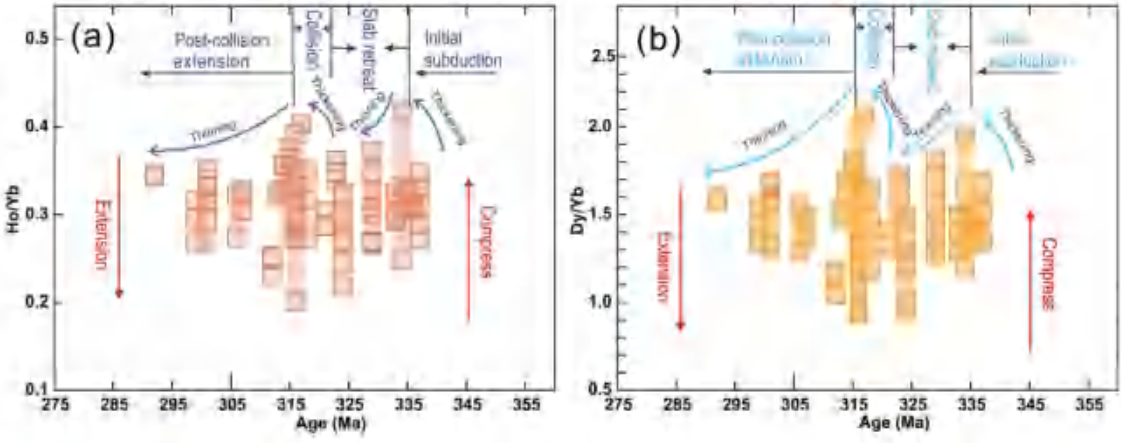

Figure 12. Age vs. Ho/Yb and Dy/Yb plots for the felsic magmatic rocks in the Aqishan-Yamansu belt. Data from Wu *et al.* (2006), Lei *et al.* (2013), Wang et al. (2016a, 2016b), Zhang *et al.* (2016), Zhang *et al.* (2017), Jiang *et al.* (2017), Lu *et al.* (2017), Zhang *et al.* (2017), Du *et al.* (2018a), and Zhao et al. (2018a, 2018b).

版权所有(C)国家科技图书文献中心 D2406250153SYJ00

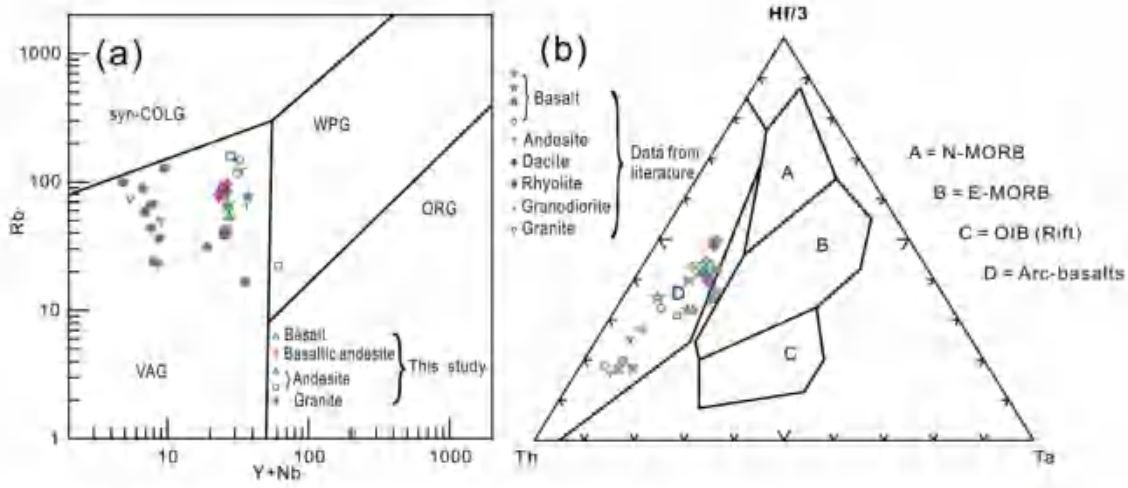

Figure 13. (a). Rb vs. Y+ Nb plot (after Pearce *et al.* 1984); (b). Th-Hf-Nb discrimination diagram (after Wood 1980).

Phase 2: a decreasing trend exhibits in the Ho/Yb and Dy/Yb ratios from ~330 to ~324 Ma, indicating the crust thickness was thinned and the melting depth was shallower. The Tugutublak basalt and basaltic andesite (~320 Ma) in this study have a depleted mantle-related source and show characteristics of subduction-related magmatic rocks, and plotted in the area of arc-basalts on the diagram of Th–Hf/3–Ta (Figure 13b). Combined with the Early Carboniferous arc-related andesite in this study, we suggested that the subduction process in the Aqishan–Yamansu Belt happened from the Early Carboniferous to the Late Carboniferous. During this process, the crustal thickness should be continuously thickened. In fact, however, the crust was thinning according to our calculation and some of the exposed rocks transmit the same information (Figure 12). The volcanic rocks of the Lower Carboniferous Yamansu Fm. Show bimodal signatures (Xiao *et al.* 1992; Xia *et al.* 2003, 2004, 2009; Hou *et al.* 2014) and have been suggested to be generated in a rift (Li *et al.* 2002). This is also supported by discovery of the 324 Ma MORB–like basalts in the Yamansu Fm. (Hou *et al.* 2014). These basalts have positive $\varepsilon_{Nd}(t)$ values (+1.4 to +5.1) and zircon $\varepsilon_{Hf}(t)$ values (+10 to +14). In combination with other geochemical characteristics, they were suggested to exhibit transitional features between island arc and mid-ocean ridge basalts and to be produced in a backarc basin (Hou *et al.* 2014; Luo *et al.* 2016). The occurrence of these MORB-like basalts represents a tectonic transition from the initial compression to the late Mississippian extension. The variation of pressure was accompanied with the crustal thinning. The absence of adakitic rocks in this period indicates that the subducted slab rollback is the most likely mechanism to account for the late Mississippian extension, which is consistent with the occurrence of the Yamansu MORB–like basalts and bimodal volcanic rocks. Therefore, a slab rollback likely occurred in the Aqishan–Yamansu Belt during the second period (Hou *et al.* 2014; Luo *et al.* 2016; Zhao et al. 2018a).

Phase 3: the increasing of Ho/Yb and Dy/Yb ratios from ~320 Ma to ~317 Ma, indicating a crustal thickening. During this period, we suppose that the variation of the crustal thickness was caused by the collision between the Dananhu–Harlik arc and the Central Tianshan Block. This collision was likely triggered by the termination of the subduction of the Kanggur ocean slab.

Phase 4: the crustal thinning during the middle to late Pennsylvanian. Compared with the early Carboniferous, the volcanic and intrusive rocks of the middle Pennsylvanian significantly reduced (Du *et al.* 2018a, 2018b). Another notable feature is the significantly elevated $\varepsilon_{Nd}(t)$ and $\varepsilon_{Hf}(t)$ values and younger Nd model ages for the Early Carboniferous magmatic rocks (Zhang *et al.* 2013, 2016; Zhou *et al.* 2010; Du *et al.* 2018a; Zhao et al., 2017, 2018), manifest that the contribution of mantle materials has increased significantly in the Late Carboniferous (Du *et al.* 2018b). This changing is also recorded by the high $\varepsilon_{Hf}(t)$ values of the granites in this study (+14.3 to +17.2) and other six Late Carboniferous granitic plutons (+3.9 to +6.8) (Zhou *et al.* 2010; Zhang *et al.* 2013, 2016; Zhao et al., 2018a, 2018b). The occurrence of the younger Hongtubao A2-type granite and the Bailingshan adakitic and E-MORB-like dykes suggests that a slab breakoff most likely happened in Late Carboniferous (Zhang *et al.* 2018; Du *et al.* 2018b; Long *et al.* 2020). Slab break-off is normally due to a decrease in the subduction rate that is damped by positive buoyancy of continental lithosphere introduced into the subduction zone (Gerya *et al.* 2004). The crustal thinning and slab

版权所有(c)国家科技图书文献中心 D2406250153SYJ00

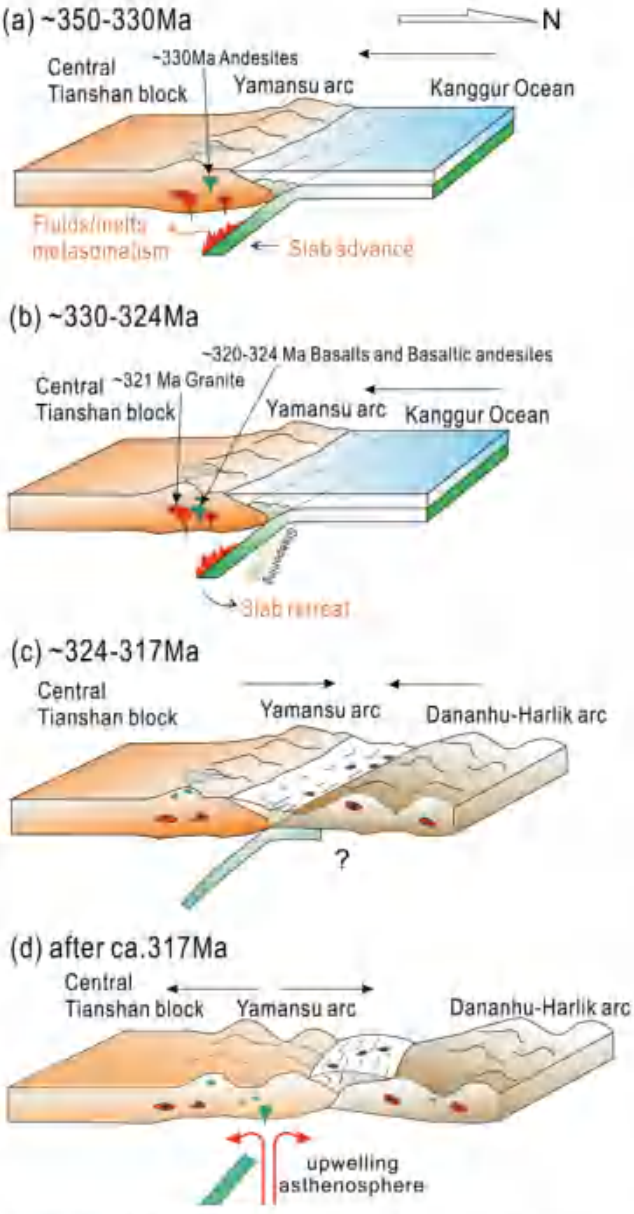

Figure 14. Carboniferous tectonic evolution for the Aqishan-Yamansu belt in Eastern Tianshan.

break-off indicate that the Aqishan–Yamansu Belt was in a tectonic setting of post-collision extension during this period.

In summary, the Carboniferous four periods of crust thickness variations in the Aqishan–Yamansu Belt had recorded the changing of subduction slab angles that caused by the transition of slab advance and retreat. An updated tectonic model, therefore, is suggested to interpret the Carboniferous tectonic evolution of the Aqishan–Yamansu Belt (Figure 14).

During the ca. 350–330 Ma, the initial formation of the Aqishan–Yamansu Belt was triggered by the southward subduction of the Kanggur ocean slab beneath the CTB (Figure 14a). As the subduction continues, slab rollback had resulted in the steepening of subduction angle and the opening of ocean basin, as well as the formation of ca. 330 Ma to 324 Ma MORB-like basalts (Figure 14b). After ca. 324 Ma, the CTB collided with the Dananhu-Harlik arc and then the oceanic basin was closed, followed by slab breakoff triggered by the increased drag force of the subducted oceanic slab (Figure 14c). The slab breakoff had caused the upwelling of asthenosphere mantle and the melting of subducted slab, and then resulted in the extension of the Aqishan–Yamansu Belt (Figure 14d).

6. Conclusions

(1) The 330 Ma Yamansu andesites were generated by partial melting of a mantle wedge metasomatized by both sediment-derived melts and slab-derived fluids.

(2) The Tugutublak basalts were derive from an enriched mantle source metasomatized by subduction-related fluids.

(3) The 321 Ma Bailingshan granites were formed by partial melting of young basaltic lower crust with limited involvement of old crustal component.

(4) The Carboniferous variation of crustal thickness in the Aqishan–Yamansu Belt experienced four periods, which were resulted from the mutual transition of slab advance and retreat.

Acknowledgments

We are grateful to the editor for the constructive comments. Financial support for this study was jointly supported by the National Key Research and Development Project (2019YFA0708601) the National Natural Science Foundation of China (41903031), and the MOST Special Fund from the State Key Laboratory of Continental Dynamics, Northwest University.

Disclosure statement

No potential conflict of interest was reported by the author(s).

Funding

This work was supported by the National Natural Science Foundation of China [41903031]; National Key Research and Development Project [2019YFA0708601].

Research Highlights:

(1) The volcanism of the Aqishan–Yamansu belt occurred at the time of ca. 348~320 Ma;
(2) The Carboniferous andesites and basalts were generated in an island arc setting;

版权所有(c)国家科技图书文献中心 D240625015355Y100

(3) The variation of crustal thickness was caused by mutual transition of slab advance and retreat.

References

Aldanmaz, E., Pearce, J.A., Thirlwall, M.F., and Mitchell, J.G., 2000, Petrogenetic evolution of late Cenozoic, post-collision volcanism in western Anatolia, Turkey: Journal of Volcanology Geothermal Research, v. 102, p. 67–95. doi:10.1016/S0377-0273(00)00182-7

Allen, M.B., Windley, B.F., and Zhang, C., 1993, Palaeozoic collisional tectonics and magmatism of the Chinese Tien Shan, Central Asia: Tectonophysics, v. 220, p. 89–115. doi:10.1016/0040-1951(93)90225-9

Ao, S.J., Mao, Q.G., Windley, B.F., Song, D.F., Zhang, Z.Y., Zhang, J.E., Wan, B., Han, C.M., and Xiao, W.J., 2021, The youngest matrix of 234 Ma of the Kanguer accretionary mélange containing blocks of N-MORB basalts: Constraints on the northward subduction of the Paleo-Asian Kanguer Ocean in the Eastern Tianshan of the southern Altaids: International Journal of Earth Sciences, v. 110, p. 791–808. doi:10.1007/s00531-021-01990-5

BGMRXUAR (Bureau of Geology and Mineral Resources of Xinjiang Uygur Autonomous Region) 1993, Regional geology of Xinjiang Uygur autonomous region, Beijing: Geological Publishing House in Chinese, p. 1–841.

Bonin, B., 2007, A-type granites and related rocks: Evolution of a concept, problems and prospects: Lithos, v. 97, p. 1–29. doi:10.1016/j.lithos.2006.12.007

Branquet, Y., Gumiaux, C., Sizaret, S., Barbanson, L., Wang, B., Cluzel, D., Li, G.R., and Delaunay, A., 2012, Synkinematic mafic/ultramafic sheeted intrusions: emplacement mechanism and strain restoration of the Permian Huangshan Ni–Cu ore belt (Eastern Tianshan, NW China): Journal of Asian Earth Sciences, v. 56, p. 240–257. doi:10.1016/j.jseaes.2012.05.021

Cai, K.D., Long, X.P., Chen, H.Y., Sun, M., and Xiao, W.J., 2017, Accretionary and collisional orogenesis in the south domain of the western Central Asian Orogenic Belt (CAOB): Journal of Asian Earth Sciences, v. 153, p. 1–8. doi:10.1016/j.jseaes.2017.11.019

Cawood, P.A., Kröner, A., Collins, W.J., Kusky, T.M., Mooney, W.D., and Windley, B.F., 2009, Accretionary orogens through Earth history, *in* Earth accretionary systems in space and time, eds., Cawood, P.A., and Kröner, A. Vol. 318, London: Geological Society of London, Special Publication, p. 1–36.

Chapman, J.B., Ducea, M.N., Decelles, P.G., and Profeta, L., 2015, Tracking changes in crustal thickness during orogenic evolution with Sr/Y: An example from the North American Cordillera: Geology, v. 43, no. 10, p. 919–922. doi:10.1130/G36996.1

Charvet, J., Laurent-Charvet, S., Faure, M., Cluzel, D., and Jong, K.D., 2011, Palaeozoic tectonic evolution of the Tianshan belt, NW China: Science China Earth Sciences, v. 54, p. 166–184. doi:10.1007/s11430-010-4138-1

Charvet, J., Shu, L.S., and Laurent-Charvet, S., 2007, Paleozoic structural and geodynamic evolution of eastern Tianshan (NW China): Welding of the Tarim and Junggar plates: Episodes, v. 30, p.162–186.

Chen, Y.J., Pirajno, F., Wu, G., Qi, J.P., and Xiong, X.L., 2012, Epithermal deposits in north Xinjiang, NW China: International Journal of Earth Sciences, v. 101, p. 889–917. doi:10.1007/s00531-011-0689-4

Collins, W.J., 2002, Hot orogens, tectonic switching, and creation of continental crust: Geology, v. 30, no. 6, p. 535–538. doi:10.1130/0091-7613(2002)030<0535:HOTSAC>2.0.CO;2

Collins, W.J., Beams, S.D., White, A.J.R., and Chappell, B.W., 1982, Nature and origin of A-type granites with particular reference to southeastern Australia: Contributions to Mineralogy and Petrology, v. 80, p. 189–200. doi:10.1007/BF00374895

Condie, K.C., 2005, TTGs and adakites: Are they both slab melts?: Lithos, v. 80, p. 33–44. doi:10.1016/j.lithos.2003.11.001

Defant, M.J., and Drummond, M.S., 1990, Derivation of some modern arc magmas by melting of young subducted lithosphere: Nature, v. 347, p. 662–665. doi:10.1038/347662a0

Dessimoz, M., Müntener, O., and Ulmer, P., 2012, A case for hornblende dominated fractionation of arc magmas: The Chelan Complex (Washington Cascades): Contributions to Mineralogy and Petrology, v. 163, no. 4, p. 567–589. doi:10.1007/s00410-011-0685-5

Dong, Y., Zhang, G., Neubauer, F., Liu, X., Hauzenberger, C., Zhou, D., and Li, W., 2011, Syn- And post-collisional granitoids in the Central Tianshan orogen: Geochemistry, geochronology and implications for tectonic evolution: Gondwana Research, v. 20, p. 568–581. doi:10.1016/j.gr.2011.01.013

Downes, H., Dupuy, C., and Leyreloup, A.F., 1990, Crustal evolution of the Hercynian belt of Western Europe: Evidence from lowercrustal granulitic xenoliths (French Massif Central): Chemical Geology, v. 83, p. 209231. doi:10.1016/0009-2541(90)90281-8

Du, L., Long, X.P., Yuan, C., Zhang, Y.Y., Huang, Z.Y., Sun, M., Wang, X.Y., and Yang, Y.H., 2018b, Mantle contribution and tectonic transition in the Aqishan–Yamansu Belt, Eastern Tianshan, NW China: Insights from geochronology and geochemistry of early carboniferous to early Permian felsic intrusions: Lithos, v. 304–307, p. 230–244. doi:10.1016/j.lithos.2018.02.010

Du, L., Long, X.P., Yuan, C., Zhang, Y.Y., Huang, Z.Y., Sun, M., and Xiao, W.J., 2018a, Petrogenesis of Late Paleozoic diorites and A-type granites in the central Eastern Tianshan, NW China: Response to post-collisional extension triggered by slab breakoff: Lithos, v. 318–319, p. 47–59. doi:10.1016/j.lithos.2018.08.006

Du, L., Long, X.P., Yuan, C., Zhang, Y.Y., Huang, Z.Y., Sun, M., Zhao, G.C., and Xiao, W.J., 2018c, Early Paleozoic dioritic and granitic plutons in the Eastern Tianshan Orogenic Belt, NW China: Constraints on the initiation of a magmatic arc in the Southern Central Asian Orogenic Belt: Journal of Asian Earth Sciences, v. 153, p. 139–153. doi:10.1016/j.jseaes.2017.03.026

Du, L., Zhu, H.L., Yuan, C., Zhang, Y.Y., Huang, Z.Y., Li, X.P., and Long, X.P., 2021, Paleozoic crustal evolution and tectonic switching in the Northeastern Tianshan: Insights from zircon Hf isotopes of granitoids: Journal of the Geological Society, v. 178, p. jgs2020–035. doi:10.1144/jgs2020-035

Gao, J., Li, M., Xiao, X., Tang, Y., and He, G., 1998, Paleozoic tectonic evolution of the Tianshan orogen, northwestern China: Tectonophysics, v. 287, p. 213–231. doi:10.1016/S0040-1951(97)00211-4

版权所有(c)国家科技图书文献中心 D2406250153SYJ00

Gao, J., Qian, Q., Long, L.L., Xi, Z., and Ji-Lei, L.I., 2009, Accretionary orogenic process of Western Tianshan, China: Geological Bulletin of China, v. 28, p.1804–1816.

Gerya, T.V., Yuen, D.A., and Maresch, W.V., 2004, Thermomechanical modelling of slab detachment: Earth and Planetary Science Letters, v. 226, p. 101–116. doi:10.1016/j.epsl.2004.07.022

Green, N.L., 2006, Influence of slab thermal structure on basalt source regions and melting conditions: REE and HFSE constraints form the Garibaldi volcanic belt, northern Cascadia subduction system: Lithos, v. 87, p. 23–49. doi:10.1016/j.lithos.2005.05.003

Griffin, W.L., Wang, X., Jackson, S.E., Pearson, N.J., O'Reilly, S.Y., Xu, X., and Zhou, X., 2002, Zircon chemistry and magma mixing, SE China: Insitu analysis of Hf isotopes, Tonglu and Pingtan igneous complexes: Lithos, v. 61, p. 237269. doi:10.1016/S0024-4937(02)00082-8

Han, C.M., Xiao, W.J., Zhao, G.C., Su, B.X., Sakyi, P.A., Ao, S., Wan, B., Zhang, J., and Zhang, Z.Y., 2014, Late Paleozoic metallogenesis and evolution of the East Tianshan Orogenic Belt (NW China, Central Asia Orogenic Belt): Geology of Ore Deposits, v. 56, p. 493–512. doi:10.1134/S1075701514060075

Hanson, G.N., and Langmuir, C.H., 1978, Modelling of major elements in mantle-melt systems using trace element approaches: Geochimica et Cosmochimica Acta, v. 42, p. 725–741. doi:10.1016/0016-7037(78)90090-X

Hawkesworth, C.J., Turner, S.P., McDermott, F., Peate, D.W., and vanCalsteren, P., 1997, U–Th isotopes in arc magmas: Implications for element transfer from the subducted crust: Science, v. 276, p. 551–555. doi:10.1126/science.276.5312.551

He, Z.Y., Zhang, Z.M., Zong, K.Q., Yu, F., and Wang, W., 2012, Zircon geochronology of Xingxingxia quartz dioritic gneisses: Implications for the tectonic evolution and Precambrian basement affinity of Chinese Tianshan orogenic belt: Acta Petrologica Sinica, v. 28, p. 1857–1874. in Chinese with English abstract

Hou, T., Zhang, Z.C., Santosh, M., Encarnacion, J., Zhu, J., and Luo, W.Q., 2014, Geochronology and geochemistry of submarine volcanic rocks in the Yamansu iron deposit, Eastern Tianshan Mountains, NW China: Constraints on the metallogenesis: Ore Geology Reviews, v. 56, p. 487–502. doi:10.1016/j.oregeorev.2013.03.008

Hu, A.Q., Jahn, B.M., Zhang, G.X., Chen, Y.B., and Zhang, Q.F., 2000, Crustal evolution and Phanerozoic crustal growth in northern Xinjiang: Nd isotopic evidence. part I. Isotopic characterization of basement rocks: Tectonophysics, v. 328, p. 15–51. doi:10.1016/S0040-1951(00)00176-1

Huang, X.W., Liang, Q.L., Gao, J.F., Liu, Y.Y., and Wang, Y.C., 2012, Geochemistry of volcanic rocks in the dikan'er formation of jueluotage region, eastern tianshan mountains and its tectonic implications: Acta Petrologica Et Mineralogica, v. 31, p. 799–817. in Chinese with English abstract

Huang, Z.Y., Long, X.P., Kröner, A., Yuan, C., Wang, Q., Sun, M., Zhao, G.C., and Wang, Y.J., 2013, Geochemistry, zircon U–Pb ages and Lu–Hf isotopes of early Paleozoic plutons in the northwestern Chinese Tianshan: Petrogenesis and geological implications: Lithos, v. 182, p. 48–66. doi:10.1016/j.lithos.2013.09.009

Huang, Z.Y., Long, X.P., Wang, X.C., Zhang, Y.Y., Du, L., Yuan, C., and Xiao, W.J., 2017, Precambrian evolution of the Chinese Central Tianshan Block: Constraints on its tectonic affinity to the Tarim Craton and responses to supercontinental cycles: Precambrian Research, v. 295, p. 24–37. doi:10.1016/j.precamres.2017.04.014

Huang, Z.Y., Yuan, C., Long, X.P., Zhang, Y.Y., and Du, L., 2019, From Breakup of Nuna to Assembly of Rodinia: A Link between the Chinese Central Tianshan Block and Fennoscandia: Tectonics, v. 38, p. 4378–4398. doi:10.1029/2018TC005471

Irvine, T.N., and Baragar, W.R.A., 1971, A guide to the chemical classification of the common volcanic rocks: Canadian Journal of Earth Sciences, v. 8, p. 523–548. doi:10.1139/e71-055

Jahn, B.M., Wu, F.Y., and Hong, D.W., 2000, Important crustal growth in the Phanerozoic: Isotopic evidence of granitoids from east-Central Asia: Journal of Earth System Science, v. 109, no. 1, p. 5–20.

Jiang, H.J., Han, J.S., Chen, H.Y., Zheng, Y., Lu, W.J., Deng, G., and Tian, Z.X., 2017, Intra-continental back-arc basin inversion and Late Carboniferous magmatism in Eastern Tianshan, NW China: Constraints from the Shaquanzi magmatic suite: Geoscience Frontiers, v. 8, p. 1447–1467. doi:10.1016/j.gsf.2017.01.008

LaFlèche, M.R., Camire, G., and Jenner, G.A., 1998, Geochemistry of post-Acadian, Carboniferous continental intraplate basalts from the Maritimes basin, Magdalen Islands, Quebec: chemical Geology, v. 148, p. 115–136. doi:10.1016/S0009-2541(98)00002-3

Langmuir, C.H., 1989, Geochemical consequences of in situ crystallization: Nature, v. 340, p. 199205. doi:10.1038/340199a0

Lei, R.X., Wu, C.Z., Gu, L.X., Zhang, Z.Z., Chi, G.X., and Jiang, Y.H., 2011, Zircon U–Pb chronology and Hf isotope of the Xingxingxia granodiorite from the Central Tianshan zone (NW China): Implications for the tectonic evolution of the southern Altaids: Gondwana Research, v. 20, p. 582–593. doi:10.1016/j.gr.2011.02.010

Lei, R.X., Wu, C.Z., Zhang, Z.Z., Gu, L.X., Tang, J.H., and Li, G.R., 2013, Geochronology, geochemistry and tectonic significances of the Yamansubei pluton in eastern Tianshan, Northwest China: Acta Petrologica Sinica, v. 29, p.2653–2664.

Li, J.Y., 2004, Late Neoproterozoic and Paleozoic tectonic framework and evolution of eastern Xinjiang, NW China: Geology Reviews, v. 50, p. 304–322. in Chinese with English abstract

Li, B., Bagas, L., Gallardo, L.A., Said, N., Diwu, C., and McCuaig, T.C., 2013, Back-arc and post-collisional volcanism in the palaeoproterozoic granites–Tanami Orogen, Australia: Precambrian Research, v. 224, p. 570–587. doi:10.1016/j.precamres.2012.11.002

Li, W.Q., Dong, F.R., and Zhou, R.H., 2000, Ophiolite discovered in Kanggurtag region and its characteristics: Xinjiang Geology, v. 18, p. 121–128. in Chinese with English abstract

Li, W.Q., Ma, H.D., Wang, R., Wang, H., and Xia, B., 2008, SHRIMP dating and Nd–Sr isotopic Tracing of Kanggurtage ophiolite in Eastern Tianshan, Xinjiang: Acta Petrologica Sinica, v. 4, p. 773–780. in Chinese with English abstract

版权所有(c)国家科技图书文献中心 D24062501535YJ00

Li, P.F., Sun, M., Shu, C.T., Yuan, C., Jiang, Y.D., Zhang, L., and Cai, K.D., 2019, Neoproterozoic-Early Paleozoic accretion to Devonian trench retreat and a comparison with Phanerozoic eastern Australia: Earth-Science Reviews, v. 198, p. 102951. doi:10.1016/j.earscirev.2019.102951

Li, J.Y., Wang, K.Z., and Li, W.Q., 2002, Tectonic evolution since the late paleozoic and mineral prospecting in eastern Tianshan Mountains, NW China: Xinjiang Geology, v. 20, p. 295–301. in Chinese with English abstract

Li, J.Y., Yang, T.N., Li, Y.P., and Zhu, Z.X., 2009, Geological features of the Karamaili faulting belt, eastern Junggar region, Xinjiang, China, and its constraints on the reconstruction of late Paleozoic ocean-continental framework of the Central Asian region: Geological Bulletin of China, v. 28, p. 1817–1826. in Chinese with English abstract

Li, Y., Yang, J.S., Zhang, J., Li, T.F., Chen, S.Y., Ren, Y.F., and Xu, X. Z., 2011, Tectonical significance of the Carboniferous volcanic rocks in eastern Tianshan: Acta Petrologica Sinica, v. 27, p. 193–209. in Chinese with English abstract

Liu, Y.J., Li, W.M., Ma, Y.F., Feng, Z.Q., Guan, Q.B., Li, S.Z., Chen, Z. X., Liang, C.Y., and Wen, Q.B., 2021. An orocline in the eastern Central Asian Orogenic Belt: Earth-Science Reviews, v. 221, p.103808.

Long, X.P., and Huang, Z.Y., 2017, Tectonic affinities of microcontinents in the Central Asian Orogenic Belt: A case study of the Chinese Tianshan Orogenic Belt: Bulletin of Mineralogy Petrology and Geochemistry, v. 36, p. 771–785. In Chinese with English abstract

Long, X.P., Wu, B., Sun, M., Yuan, C., Xiao, W.J., and Zuo, R., 2020, Geochronology and geochemistry of Late Carboniferous dykes in the Aqishan–Yamansu Belt, eastern Tianshan: Evidence for a post-collisional slab breakoff: Geoscience Frontiers, v. 11, p. 347–362. doi:10.1016/j.gsf.2019.06.003

Long, X.P., Yuan, C., Sun, M., Xiao, W.J., Wang, Y.J., Cai, K.D., and Jiang, Y.D., 2012, Geochemistry and Nd isotopic composition of the early Paleozoic flysch sequence in the Chinese Altai, Central Asia: Evidence for a northward-derived mafic source and insight into Nd model ages in accretionary orogen: Gondwana Research, v. 22, p. 554–566. doi:10.1016/j.gr.2011.04.009

Lu, W.J., Chen, H.Y., Zhang, L., Han, J.S., Xiao, B., Li, D.F. et al. 2017, Age and geochemistry of the intrusive rocks from the shaquanzi–hongyuan Pb–Zn mineral district: Implications for the late carboniferous tectonic setting and pb–zn mineralization in the eastern tianshan, nw China: Lithos, doi:10.1016/j.lithos.2017.10.009

Luo, T., Liao, A.Q., Chen, J.P., Zhang, X.H., Guo, D.B., and Hu, Z.C., 2012, LA-ICP-MS zircon U- Pb dating of the volcanic rocks from Yamansu Formation in the Eastern Tianshan, and its geological significance: Earth Science-Journal of China University of Geosciences, v. 6, p. 1338–1352. in Chinese with English abstract

Luo, T., Liao, Q.A., Zhang, X.H., Chen, J.P., Wang, G.C., and Huang, X., 2016, Geochronology and geochemistry of Carboniferous metabasalts in eastern Tianshan, Central Asia: Evidence of a back-arc basin: International Geology Review, v. 58, p. 756–772. doi:10.1080/00206814.2015.1114433

Ma, R.S., Shu, L.S., and Sun, J., 1997, Tectonic Evolution and Metallogeny of Eastern Tianshan Mountains,Geological Publishing House Beijing. p. 202.

Mamani, M., Worner, G., and Sempere, T., 2010, Geochemical variations in igneous rocks of the central Andean orocline (13° S to 18°S): Tracing crustal thickening and magma generation through time and space: Geological Society of America Bulletin, v. 122, no. 1–2, p. 162–182. doi:10.1130/B26538.1

Maniar, P.D., and Piccoli, P.M., 1989, Tectonic discrimination of granitoids: Geological Society of American Bulletin, v. 101, p. 635–643. doi:10.1130/0016-7606(1989)101<0635:TDOG>2.3.CO;2

Mao, Q.G., Ao, S.J., Windley, B.F., Zhang, Z.Y., Song, D.F., Zhang, J.E., Wan, B., Tan, W., Han, C.M., and Xiao, W.J., 2021, Petrogenesis of Late Carboniferous-Early Permian mafic-ultramafic-felsic complexes in the eastern Central Tianshan, NW China: The result of subduction-related transtension?: Gondwana Research, v. 95, p. 72–87. doi:10.1016/j.gr.2021.03.007

Mao, Y.J., Tang, D.M., Qin, K.Z., and Taranovic, V., 2016, Geochemistry of the ~326 Ma Xinyuan mafic intrusion in the Eastern Junggar Terrane, Northwest China: Implications for tectonic setting and magmatic Ni–Cu mineralization potential: International Geology Review, v. 6, p. 1276–1291.

Mao, Q.G., Wang, J.B., Xiao, W.J., Windley, B.F., Schulmann, K., Yu, M.J., Fang, T.H., and Li, Y.C., 2019, Mineralization of an intra-oceanic arc in an accretionary orogen: Insights from the early Silurian Honghai VMS Cu-Zn deposit and associated adakites of the Eastern Tianshan (NW China): Geological Society of America Bulletin, v. 131, p. 803–830. doi:10.1130/B31986.1

Mcculloch, M.T., and Gamble, J.A., 1991, Geochemical and Geodynamical Constraints on Subduction Zone Magmatism: Earth and Planetary Science Letters, v. 102, p. 358–374. doi:10.1016/0012-821X(91)90029-H

Middlemost, E.A.K., 1994, Naming materials in the magma/igneous rock system: Earth-Science Reviews, v. 37, p. 215–224. doi:10.1016/0012-8252(94)90029-9

Miyashiro, A., 1974, Volcanic rock series in island arcs and active continental margins: American Journal of Science, v. 274, p. 321–355. doi:10.2475/ajs.274.4.321

Niu, Y.L., 2010, Some basic concepts and problems on the petrogenesis of intra-plate ocean island basalts: Chinese Science Bulletin, v. 55, p. 103–114. in Chinese

Pearce, J.A., 2008, Geochemical fingerprinting of oceanic basalts with applications to ophiolite classification and the search for Archean oceanic crust: Lithos, v. 100, p. 14–48. doi:10.1016/j.lithos.2007.06.016

Pearce, J.A., Harris, N.B.W., and Tindle, A.G., 1984, Trace element discrimination diagrams for the tectonic interpretation of granitic rocks: Journal of Petrology, v. 25, p. 956–983. doi:10.1093/petrology/25.4.956

Pearce, J.A., Stern, J.R., Bloomer, S.H., and Fryer, P., 2005, Geochemical mapping of the Mariana arc-basin system: Implications for the nature and distribution of subduction components: Geochemistry Geophysics Geosystems, v. 6, doi:10.1029/2004GC000895

Peccerillo, A., Barberio, M.R., Yirgu, G., Ayalew, D., Barbieri, M., and Wu, T.W., 2003, Relationships between Mafic and Peralkaline Silicic Magmatism in Continental Rift settings: A Petrological, Geochemical and Isotopic study of the Gedemsa Volcano: Central Ethiopian Rift. Journal of Petrology, v. 44, p.2003–2032.

版权所有(c)国家科技图书文献中心 D2406250153SYJ00

Peccerillo, A., and Taylor, S.R., 1976, Geochemistry of eocene calc-alkaline volcanic rocks from the Kastamonu area, Northern Turkey: Contributions to Mineralogy & Petrology, v. 58, p. 63–81. doi:10.1007/BF00384745

Petford, N., and Gallagher, K., 2001, Partial melting of mafic (amphibolitic) lower crust by periodic influx of basaltic magma: Earth and Planetary Science Letters, v. 193, p. 483499. doi:10.1016/S0012-821X(01)00481-2

Plank, T., and Langmuir, C.H., 1998, The chemical composition of subducting sediment and its consequences for the crust and mantle: Chemical Geology, v. 145, p. 325–394. doi:10.1016/S0009-2541(97)00150-2

Qin, K.Z., Fang, T.H., and Wang, S.L., 2002, Plate tectonics division, evolution and metallogenic settings in eastern Tianshan mountains, NWChina: Xinjiang Geology, v. 20, p. 302–308. in Chinese with English abstract

Rapp, R.P., Shimizu, N., Norman, M.D., and Applegate, G.S., 1999, Reaction between slab-derived melts and peridotite in the m antle wedge: Experimental constraints at 3.8 GPa: Chemical Geology, v. 160, p. 335–356. doi:10.1016/S0009-2541(99)00106-0

Rhea, K.W., and Stanley, R.H., 2005, Major and trace element composition of the depleted MORB mantle (DMM): Earth and Planetary Science Letters, v. 231, p. 53–72. doi:10.1016/j.epsl.2004.12.005

Richards, J.P., and Kerrich, R., 2007, Special paper: Adakitelike rocks: Their diverse origins and questionable role in metallogenesis: Economic Geology, v. 102, p. 537–576. doi:10.2113/gsecongeo.102.4.537

Rollinson, H.R., 1993, Using Geochemical Data: Evaluation, Presentation, Interpretation,Essex: Longman Scientific and Technical, Longman Singapore Publishers (Pte) Ltd Singapore. 1–352 p.

Royden, L.H., 1993, The tectonic expression slab pull at continental convergent boundaries: Tectonics, v. 12, no. 2, p. 303–325. doi:10.1029/92TC02748

Rudnick, R.L., and Gao, S., 2003, Composition of the continental crust: Treatise on Geochemistry, v. 3, p.1–64.

Safonova, I., Kotlyarov, A., Krivonogov, S., and Xiao, W., 2017, Intra-oceanic arcs of the Paleo-Asian Ocean: Gondwana Research, v. 50, p. 167–194. doi:10.1016/j.gr.2017.04.005

Sengör, A.M.C., Natalin, B.A., and Burtman, V.S., 1993, Evolution of the Altaid tectonic collage and Palaeozoic crustal growth in Eurasia: Nature, v. 364, p. 299–307. doi:10.1038/364299a0

Shu, L.S., Chen, Y., Lu, H.F., Charvet, J., Laurent-Charvet, S., and Yin, D.H., 2000, Paleozoic accretionary terranes in Northern Tianslian, NW China: Chinese Journal of Geochemistry, v. 19, no. 3, p. 193–202. doi:10.1007/BF03166877

Shu, L.S., Jacques, C., Lingzhi, G., Huafu, H.F., and Sebastien, L.-C., 1999, A Large-Scale Palaeozoic Dextral Ductile Strike-Slip Zone: The Aqqikkudug-Weiya Zone along the Northern Margin of the Central Tianshan Belt, Xinjiang, NW China: Acta Geologica Sinica - English Edition, v. 73, p. 148–162. doi:10.1111/j.1755-6724.1999.tb00822.x

Shu, L.S., Yu, J.H., Charvet, J., Laurent-Charvet, S., Sang, H.Q., and Zhang, R.G., 2004, Geological, geochronological and geochemical features of granulites in the Eastern Tianshan, NW China: Journal of Asian Earth Sciences, v. 24, p. 25–41. doi:10.1016/j.jseaes.2003.07.002

Shuto, K., Sato, M., Kawabata, H., Osanai, Y., Nakano, N., and Yashima, R., 2013, Petrogenesis of Middle Miocene Primitive Basalt, Andesite and Garnet-bearing Adakitic Rhyodacite from the Ryozen Formation: Implications for the Tectonomagmatic Evolution of the NE Japan Arc: Journal of Petrology, v. 54, no. 12, p. 2413–2454. doi:10.1093/petrology/egt052

Stern, C.R., and Kilian, R., 1996, Role of the subducted slab, mantle wedge and continental crust in the generation of adakites from the Andean Austral Volcanic Zone: Contributions to Mineralogy and Petrology, v. 123, no. 3, p. 263–281. doi:10.1007/s004100050155

Su, C.Q., Jiang, C.Y., and Xia, M.Z., 2009, Geochemistry and zircons SHRIMP UPb age of volcanic rocks of Aqishan formation in the eastern area of north Tianshan, China: Acta Petrologca Sinica, v. 25, p. 901–915. in Chinese with English abstract

Su, B.-X., Qin, K.-Z., Sakyi, P.A., Malaviarachchi, S.P.K., Liu, -P.-P., Tang, D.-M., Xiao, Q.-H., Sun, H., Ma, Y.-G., and Mao, Q., 2012b, Occurrence of an Alaskan-type complex in the Middle Tianshan Massif, Central Asian Orogenic Belt: Inferences from petrological and mineralogical studies: International Geology Review, v. 54, p. 249–269. doi:10.1080/00206814.2010.543009

Su, Y.P., Zheng, J.P., Griffin, W.L., Zhao, J.H., Tang, H.Y., Ma, Q., and Lin, X.Y., 2012, Geochemistry and geochronology of Carboniferous volcanic rocks in the eastern Junggar terrane, NW China: Implication for a tectonic transition: Gondwana research, v. 22, p. 1009–1029. doi:10.1016/j.gr.2012.01.004

Sun, -S.-S., and McDonough, W.F., 1989, Chemical and isotopic systematics of oceanic basalts: Implications for mantle composition and processes: Geological Society, London, Special Publications, v. 42, p. 313–345. doi:10.1144/GSL.SP.1989.042.01.19

Tang, G.-J., Chung, S.-L., Hawkesworth, C.J., Cawood, P.A., Wang, Q., Wyman, D.A., Xu, Y.-G., and Zhao, Z.-H., 2017, Short episodes of crust generation during protracted accretionary processes: Evidence from Central Asian Orogenic Belt, NW China: Earth and Planetary Science Letters, v. 464, p. 142–154. doi:10.1016/j.epsl.2017.02.022

Tang, G.J., Chung, S.-L., Wang, Q., Wyman, D.A., Dan, W., Chen, H.-Y., and Zhao, Z.-H., 2014, Petrogenesis of a Late Carboniferous mafic dike–granitoid association in the western Tianshan: Response to the geodynamics of oceanic subduction: Lithos, v. 202-203, p. 85–99. doi:10.1016/j.lithos.2014.04.010

Tao, Z., Yin, J.Y., Sun, M., Wang, T., Yuan, C., Chen, W., Huang, H., Seltmann, R., Thomson, S.N., and Chen, Y.L., 2022, Spatial and temporal variations of geochemical and isotopic compositions of Paleozoic magmatic rocks in the Western Tianshan, NW China: A magmatic response of the Advancing and Retreating Subduction: Journal of Asian Earth Sciences, v. 105112 doi:10.1016/j.jseaes.2022.105112

Villagómez, D., Spikings, R., Magna, T., Kammer, A., Winkler, W., and Beltrán, A., 2011, Geochronology, geochemistry and tectonic evolution of the Western and Central cordilleras of Colombia: Lithos, v. 125, p. 875–896. doi:10.1016/j.lithos.2011.05.003

Wang, B., Chen, Y., Zhan, S., Shu, L.S., Faure, M., Cluzel, D., Charvet, J., and Laurent-Charvet, S., 2007, Primary Carboniferous and Permian paleomagnetic results from the yili block (NW China)

版权所有(c)国家科技图书文献中心 D2406250153SYJ00

and their implications on the geodynamic evolution of Chinese tianshan belt: Earth and Planetary Science Letters, v. 263, p. 288–308. doi:10.1016/j.epsl.2007.08.037

Wang, B., Cluzel, D., Jahn, B.-M., Shu, L.S., Chen, Y., Zhai, Y.Z., Branquet, Y., Barbanson, L., and Sizaret, S., 2014, Late paleozoic pre- and syn-kinematic plutons of the kangguer-huangshan shear zone: Inference on the tectonic evolution of the eastern Chinese North Tianshan: American Journal of Science, v. 314, p. 43–79. doi:10.2475/01.2014.02

Wang, L.S., Li, H.Q., Chen, Y.C., Liu, D.Q., 2005, Geological feature andmineralization epoch of Bailingshan iron deposit, Hami, Xingjiang, China: Mineral Deposits, v. 24, p. 280–284. in Chinese with English abstract

Wang, Y., Li, J., and Sun, G., 2008, Postcollisional Eastward Extrusion and Tectonic Exhumation along the Eastern Tianshan Orogen, Central Asia: Constraints from dextral strike-slip motion and 40Ar/39Ar geochronological evidence: The Journal of Geology, v. 116, no. 6, p. 599–618. doi:10.1086/591993

Wang, B., Shu, L.S., Faure, M., Jahn, B.-M., Cluzel, D., Charvet, J., Chung, S.-L., and Meffre, S., 2011, Paleozoic tectonics of the southern Chinese Tianshan: Insights from structural, chronological and geochemical studies of the Heiyingshan ophiolitic mélange (NW China): Tectonophysics, v. 497, p. 85–104. doi:10.1016/j.tecto.2010.11.004

Wang, H., Wu, Y.-B., Qin, Z.-W., Zhu, L.-Q., Liu, Q., Liu, X.-C., Gao, S., Wijbrans, J.R., Zhou, L., and Gong, H.-J., 2013, Age and geochemistry of Silurian gabbroic rocks in the Tongbai orogen, central China: Implications for the geodynamic evolution of the North Qinling arc–back-arc system: Lithos, v. 179, p. 1–15. doi:10.1016/j.lithos.2013.07.021

Wang, Y.-H., Xue, C.-J., Gao, J.-B., Zhang, -F.-F., Liu, -J.-J., Wang, J.-P., and Wang, J.-C., 2016a, The genesis of the ores and granitic rocks at the hongshi Au deposit in eastern tianshan, China: Constraints from zircon u–pb geochronology, geochemistry and isotope systematics: Ore Geology Reviews, v. 74, p. 122–138. doi:10.1016/j.oregeorev.2015.11.018

Wang, Y.-H., Xue, C.-J., Liu, -J.-J., Wang, J.-P., Yang, J.-T., Zhang, -F.-F., Zhao, Z.-N., Zhao, Y.-J., and Liu, B., 2015, Early carboniferous adakitic rocks in the area of the Tuwu deposit, Eastern Tianshan, NW China: Slab melting and implications for porphyry copper mineralization: Journal of Asian Earth Sciences, v. 103, p. 332–349. doi:10.1016/j.jseaes.2014.09.032

Wang, B., Zhai, Y.Z., Kapp, P., De Jong, K., Zhong, L.L., Liu, H.S., Ma, Y.Z., Gong, H.J., and Geng, H.Y., 2018, Accretionary tectonics of back-arc oceanic basins in the South Tianshan: Insights from structural, geochronological, and geochemical studies of the Wuwamen ophiolite mélange: Geological Society Of America Bulletin, v. 130, p. 581–582. doi:10.1130/B31397.1

Wang, Y.H., Zhang, F.F., Liu, J.J., and Que, C.Y., 2016b, Carboniferous magmatism and mineralization in the area of the Fuxing Cu deposit, Eastern Tianshan, China: Evidence from zircon U–Pb ages, petrogeochemistry, and Sr–Nd–Hf–O isotopic compositions: Gondwana Research, v. 34, p. 109–128. doi:10.1016/j.gr.2016.03.007

Whalen, J.B., Currie, K.L., and Chappell, B.W., 1987, A-type granites: Geochemical characteristics, discrimination and petrogenesis: Geochemical Characteristics, Discrimination and petrogenesis.Contributions to Mineralogy and Petrology, v. 95, p. 407–419. doi:10.1007/BF00402202

Wilhem, C., Windley, B.F., and Stampfli, G.M., 2012, The Altaids of Central Asia: A tectonic and evolutionary innovative review: Earth-Science Reviews, v. 113, p. 303–341.

Wilkinson, J.F.G., and Le Maitre, R.W., 1987, Upper mantle amphiboles and Micas and TiO_2, K_2O, and P_2O5 Abundances and 100 Mg/(Mgþ Fe2þ) Ratios of Common Basalts and Andesites: Implications for modal mantle metasomatism and undepleted mantle compositions: Journal of Petrology, v. 28, p. 37–73. doi:10.1093/petrology/28.1.37

Windley, B.F., Alexeiev, D., Xiao, W., Kroner, A., and Badarch, G., 2007, Tectonic models for accretion of the Central Asian Orogenic Belt: Journal of the Geological Society, v. 164, p. 31–47. doi:10.1144/0016-76492006-022

Windley, B.F., Allen, M.B., Zhang, C., Zhao, Z.Y., and Wang, G.R., 1990, Paleozoic accretion and Cenozoic redeformation of the Chinese Tien Shan Range, Central Asia: Geology, v. 18, p. 128–131. doi:10.1130/0091-7613(1990)018<0128:PAACRO>2.3.CO;2

Wood, D.A., 1980, The application of a ThHfTa diagram to problems of tectonomagmatic classification and to establishing the nature of crustal contamination of basaltic lavas of the British Tertiary Volcanic province: Earth and Planetary Science Letters, v. 50, p. 11–30. doi:10.1016/0012-821X(80)90116-8

Woodhead, J.D., Hergt, J.M., Davidson, J.P., and Eggins, S.M., 2001, Hafnium isotope evidence for 'conservative' element mobility during subduction zone processes: Earth and Planetary Science Letters, v. 192, p. 331–346. doi:10.1016/S0012-821X(01)00453-8

Wu, C.Z., Zhang, Z.Z., Zaw, K., Della-Pasque, F., Tang, J.H., Zheng, Y.C., Wang, C.S., and San, J.Z., 2006, Geochronology, geochemistry and tectonic significances of the Hongyuntan granitoids in the Qoltag area, Eastern Tianshan: Acta Petrologica Sinica, v. 22, p. 1121–1134. in Chinese with English abstract

Xia, L.Q., Xia, Z.C., and Xu, X.Y., 2009, Do the Tianshan carboniferous volcanic successions contain Nb-enriched arc basalts?: Earth Science Frontiers (China University of Geosciences (Beijing)), v. 16, p. 303–317. in Chinese with English abstract

Xia, L.Q., Xu, X.Y., Xia, Z.C., Li, X.M., Ma, Z.P., and Wang, L.S., 2004, Petrogenesis of Carboniferous rift-related volcanic rocks in the Tianshan, northwestern China: Geological Society of America Bulletin, v. 116, p. 419–433. doi:10.1130/B25243.1

Xia, L.Q., Xue, X.Y., Xia, Z.C., Xiangmin, L.I., Zhongping, M.A., and Lishe, W., 2003, Carboniferous post-collisional Rift Volcanism of the Tianshan Mountains, Northwestern China: Acta Geologica Sinica - English Edition, v.77, p. 338–360. in Chinese with English abstract doi:10.1111/j.1755-6724.2003.tb00751.x

Xiao, W.J., Huang, B.C., Han, C.M., Sun, S., and Li, J.L., 2010, A review of the western part of the Altaids: A key to understanding the architecture of accretionary orogens: Gondwana Research, v. 18, p. 253–273. doi:10.1016/j.gr.2010.01.007

Xiao, W.J., and Santosh, M., 2014, The western Central Asian Orogenic Belt: A window to accretionary orogenesis and continental growth: Gondwana Research, v. 25, p. 1429–1444. doi:10.1016/j.gr.2014.01.008

Xiao, X.C., Tang, Y.Q., Feng, Y.M., Zhu, B.Z., Li, J., and Zhao, M., 1992, The Tectonic evolution of North Xinjiang and its adjacent regions, Beijing Geological Publishing House, p. 190. in Chinese with English abstract

版权所有(c)国家科技图书文献中心 D2406250153SYJ001

Xiao, W.J., Windley, B.F., Allen, M.B., and Han, C.M., 2013, Paleozoic multiple accretionary and collisional tectonics of the Chinese Tianshan orogenic collage: Gondwana Research, v. 23, p.1316–1341.

Xiao, W.J., Windley, B.F., Han, C.M., Liu, W., Wan, B., Zhang, J.E., Ao, S.J., Zhang, Z.Y., and Song, D.F., 2018, Late Paleozoic to early Triassic multiple roll-back and oroclinal bending of the Mongolia collage in Central Asia: Earth-Science Reviews, v. 186, p.94–128.

Xiao, W.J., Windley, B.F., Sun, S., Li, J., Huang, B.C., Han, C.M., Yuan, C., Sun, M., and Chen, H.L., 2015, A Tale of Amalgamation of Three Permo-Triassic Collage Systems in Central Asia: Oroclines, Sutures, and Terminal Accretion: Annual Review of Earth and Planetary Sciences, v. 43, p. 477–507. doi:10.1146/annurev-earth-060614-105254

Xiao, W.J., Windley, B.F., Yuan, C., Sun, M., Han, C.M., Lin, S.F., Chen, H.L., Yan, Q.R., Liu, D.Y., Qin, K.Z., Li, J.L., and Sun, S., 2009, Paleozoic multiple subduction-accretion processes of the southern Altaids: American Journal of Science, v. 309, p. 221–270. doi:10.2475/03.2009.02

Xiao, W.J., Zhang, L.C., Qin, K.Z., Sun, S., and Li, J.L., 2004, Paleozoic accretionary and collisional tectonics of the Eastern Tianshan (China): Implications for the continental growth of Central Asia: American Journal of Science, v. 304, p. 370–395. doi:10.2475/ajs.304.4.370

Xu, X.W., Ma, T.L., Sun, L.Q., and Cai, X.P., 2003, Characteristics and dynamic origin of the large-scale Jiaoluotage ductile compressional zone in the eastern Tianshan Mountains, China: Journal of Structural Geology, v. 25, no. 11, p. 1901–1915. doi:10.1016/S0191-8141(03)00017-8

Yuan, F., Zhou, T.F., Fan, Y., Tan, L.G., Cooke, D., Meffre, S., and Wang, W.J., 2007, LA-ICPMS U-Pb age of zircon from basalt of Matoutan group in Shilipo native copper mineralized area, eastern Tianshan, Xinjiang: Acta Petrologica Sinica, v. 23, p. 1973–1980. in Chinese with English abstract

Zhang, W.F., Chen, H.Y., Han, J.S., Zhao, L.D., Huang, J.H., Yang, J.T., and Yan, X.L., 2016, Geochronology and geochemistry of igneous rocks in the Bailingshan area: Implications for the tectonic setting of late Paleozoic magmatism and iron skarn mineralization in the eastern Tianshan, NW China: Gondwana Research, v. 38, p. 0–59. doi:10.1016/j.gr.2015.10.011

Zhang, W.F., Chen, H.Y., Jiang, H.J., Lu, W.J., Liang, P., Xu, C., Yan, X.L., and Yang, J.T., 2017, Geochronology, geochemistry and petrogenesis of granitoids in the Duotoushan Fe-Cu deposit, Eastern Tianshan, Xinjiang province: Implications on tectonic setting of late Paleozoic magmatism: Geotectonica Et Metallogenia, v. 14, p. 1171–1191. in Chinese with English abstract

Zhang, X.H., Huang, X., Chen, J.P., Liao, Q.A., and Duan, X.F., 2012b, Stratigraphic sequence of carboniferous marine volcanic-deposit rock and its geological age in Juotage Area, Eastern Tianshan: Earth Science-Journal of China University of Geosciences, v. 6, p. 1305–1314. in Chinese with English abstract

Zhang, Y.Y., Sun, M., Yuan, C., Long, X.P., Jiang, Y.D., Li, P., Huang, Z.Y., and Du, L., 2018, Alternating trench advance and retreat: Insights from Paleozoic magmatism in the eastern Tianshan: Central Asian Orogenic Belt. Tectonics, v. 37, p.2142–2164.

Zhang, X.R., Zhao, C.G., Eizenhöfer, P.R., Sun, M., Han, Y.G., Hou, W.Z., Liu, D.X., Wang, B., Liu, Q., and Xu, B., 2015, Latest Carboniferous closure of the Junggar Ocean constrained by geochemical and zircon U–Pb–Hf isotopic data of granitic gneisses from the Central Tianshan block, NW China: Lithos, v. 238, p. 26–36. doi:10.1016/j.lithos.2015.09.012

Zhang, X.R., Zhao, G.C., Han, Y.G., and Sun, M., 2019, Differentiating advancing and retreating subduction zones through regional zircon Hf isotope mapping: A Case Study from the Eastern Tianshan, v. 66, p. 246–254. NW China. Gondwana Research

Zhang, D.Y., Zhou, T.F., Yuan, F., Fiorentini, M.L., Said, N., Lu, Y.J., and Pirajno, F., 2013, Geochemical and isotopic constraints on the genesis of the Jueluotage native copper mineralized basalt, Eastern Tianshan, Northwest China: Journal of Asian Earth Sciences, v. 73, p. 317–333. doi:10.1016/j.jseaes.2013.04.043

Zhang, D.Y., Zhou, T.F., Yuan, F., Liu, S., Lu, Y.J., Xu, C., and Ning, F.Q., 2012a, Geochronology and geological indication of the native copper mineralized basalt formation in Jueluotage area, Eastern Tianshan, Xinjiang: Acta Petrologica Sinica, v. 28, p. 2392–2400. in Chinese with English abstract

Zhao, L.D., Chen, H.Y., Han, J.S., and Zhang, S.L., 2021, Carboniferous high-Mg andesitic and dioritic rocks in the Aqishan–Yamansu belt: Implications for mantle metasomatism and tectonic setting of the Eastern Tianshan: Journal of Asian Earth Sciences, v. 219, p. 104887. doi:10.1016/j.jseaes.2021.104887

Zhao, L.D., Chen, H.Y., Hollings, P., and Han, J.S., 2018a, Late Paleozoic magmatism and metallogenesis in the Aqishan–Yamansu Belt, Eastern Tianshan: Constraints from the Bailingshan intrusive complex: Gondwana Research, v. 65, p. 68–85. doi:10.1016/j.gr.2018.08.004

Zhao, L.D., Chen, H.Y., Zhang, L., Zhang, W.F., Yang, J.T., and Yan, X.L., 2018b, The Late Paleozoic magmatic evolution of the Aqishan–Yamansu belt, Eastern Tianshan: Constraints from geochronology, geochemistry and Sr–Nd–Pb–Hf isotopes of igneous rocks: Journal of Asian Earth Sciences, v. 153, p. 170–192. doi:10.1016/j.jseaes.2017.07.038

Zheng, Y.F., 2012, Metamorphic chemical geodynamics in continental subduction zones: Chemical Geology, v. 328, p.5–48.

Zheng, R.Q., 2015, Geological characteristics and genesis of Hongyuntan iron deposits in the Eastern Tianshan, Xinjiang China University of Geosciences (Beijing) 1–102 p. in Chinese with English abstract

Zhou, T.F., Yuan, F., Zhang, D.Y., Fan, Y., Liu, S., Peng, M.X., and Zhang, J.D., 2010, Geochronology, tectonic setting and mineralization of granitoids in Jueluotage area, eastern Tianshan, Xinjiang: Acta Petrologica Sinica, v. 26, p. 478–502. in Chinese with English abstract

Zhu, D.C., Pan, G.T., Zhao, Z.D., Lee, H.Y., Kang, Z.Q., Liao, Z.L., Wang, L.Q., Li, G.M., Dong, G.C., and Liu, B., 2009, Early Cretaceous subduction-related adakite-like rocks in the Gangdese, south Tibet: Products of slab melting and subsequent melt–peridotite interaction: Journal of Asian Earth sciences, v. 34, p. 298–309. doi:10.1016/j.jseaes.2008.05.003

版权所有(c)国家科技图书文献中心 D2406250153SYJ00